not further reduce their body temperatures under the fed condition (Figure 3I, left panel). We next examined the effect of cold exposure on 24 hr fasted mice. Unlike with 48 hr fasting, under 24 hr fasting conditions, *AceCS2*$^{-/-}$ mice maintained their core body temperatures at levels similar to *AceCS2*$^{+/+}$ mice, although both levels were equally reduced by 2°C–3°C compared to fed levels. Exposure of these mice to cold further decreased their core temperatures; however, after 5 hr cold exposure, there was no significant difference between *AceCS2*$^{-/-}$ and *AceCS2*$^{+/+}$ mice (Figure 3I, right panel). These data indicate that adaptive thermogenesis in response to low temperature was not impaired in *AceCS2*$^{-/-}$ mice and further suggest that the sympathetic nervous system is able to properly maintain core body temperature in *AceCS2*$^{-/-}$ mice.

We hypothesized that fasting *AceCS2*$^{-/-}$ mice would lead to decreased exercise tolerance, owing to impaired acetate oxidation and subsequent reduction of ATP production in skeletal muscle (Figure 3E). *AceCS2*$^{-/-}$ mice were exercised on a motorized treadmill apparatus using a run-to-exhaustion protocol. *AceCS2*$^{-/-}$ mice fasted for 48 hr exhibited a markedly reduced capacity to sustain running exercise, whereas the running capacity of *AceCS2*$^{+/+}$ mice did not change between the fed and fasted conditions (Figure 3J). This suggests that acetate is an important fuel required for exercise as well as for heat generation during fasting.

AceCS2$^{-/-}$ Mice Compensate for Metabolic Acidosis through Hyperventilation

Because the plasma acetate levels are very high in *AceCS2*$^{-/-}$ mice, we speculated that these mice could be acidotic, and, if not, they might be hyperventilating to blow off CO_2 to prevent acidemia. Accordingly, we measured the arterial blood gases, pH, and bicarbonate concentration. The values of arterial carbon dioxide partial pressure ($PaCO_2$) were significantly decreased in *AceCS2*$^{-/-}$ mice ($p < 0.05$, $n = 5–6$), indicating that *AceCS2*$^{-/-}$ mice were hyperventilating to blow off CO_2. There were no significant differences in the values of PaO_2, standardized bicarbonate concentration ($[HCO_3^-]$), and the pH (Table 1). These data indicate that *AceCS2*$^{-/-}$ mice were hyperventilating to compensate for a possible acidosis caused by acetate accumulation. This hyperventilation in *AceCS2*$^{-/-}$ mice might account for some of their increased energy expenditure compared to *AceCS2*$^{+/+}$ mice.

AceCS2$^{-/-}$ Mice Exhibit Hypothermia and Hypoglycemia under Low-Carbohydrate, High-Fat Diet

Similar to fasting conditions, we hypothesized that acetate utilization may be important under low-glucose or low-carbohydrate intake states. To examine this possibility, 4-week-old *AceCS2*$^{-/-}$ and *AceCS2*$^{+/+}$ mice were fed a low-carbohydrate, high-fat diet (LC/HF; 0.4% carbohydrate, 90.5% fat, and 9.1% protein from calories). At the time of weaning (4 weeks of age), *AceCS2*$^{-/-}$ mice weighed an average of 40% less than their littermates (Figures S1A–S1C), and plasma acetate levels were markedly elevated (Figure 4A). Plasma ketone bodies, NEFA, glucose, and insulin levels were comparable between *AceCS2*$^{+/+}$ and *AceCS2*$^{-/-}$ mice (Table S1).

On LC/HF diet, *AceCS2*$^{-/-}$ mice exhibited lower body temperatures (Figure 4B). This was most severe (30.1 ± 1.4°C) on day 2 of LC/HF diet feeding, whereas *AceCS2*$^{+/+}$ mice maintained their body temperatures at 37°C on this diet. In addition, *AceCS2*$^{-/-}$ mice lost weight, whereas the body weight of *AceCS2*$^{+/+}$ mice remained stable (Figure 4C). Furthermore, *AceCS2*$^{-/-}$ mice had sustained hypoglycemia (56 ± 5 mg/dl) over this period compared to *AceCS2*$^{+/+}$ mice that exhibited transiently decreased plasma glucose levels at weaning but soon recovered to normal levels (137 ± 7 mg/dl) (Figure 4D). This transient hypoglycemia in *AceCS2*$^{+/+}$ is most likely from the stress of forced weaning, which causes suppression of feeding on the day of weaning. Plasma NEFA and ketone body levels were highly elevated, but there were no significant differences between *AceCS2*$^{+/+}$ and *AceCS2*$^{-/-}$ mice except in ketone body levels on day 3 of the LC/HF diet (Figures 4E and 4F). The abundance of mRNAs for the enzymes involved in gluconeogenesis was not decreased in *AceCS2*$^{-/-}$ mice compared to *AceCS2*$^{+/+}$ mice (Figure S3A). Furthermore, injection of pyruvate to these mice rescued hypoglycemia (Figure S3B), indicating that the gluconeogenic pathway is intact.

Table 1. Blood Gas Analysis of *AceCS2*$^{+/+}$ and *AceCS2*$^{-/-}$ Mice

	+/+	−/−
pH	7.34 ± 0.03	7.34 ± 0.03
PaO_2 (mm Hg)	102.3 ± 2.7	108.8 ± 5.5
$PaCO_2$ (mm Hg)	37.3 ± 1.2	33.3 ± 0.9[a]
HCO_3^- (mM)	19.7 ± 0.8	17.6 ± 1.3
BE (mM)	−5.1 ± 1.2	−6.9 ± 1.9

Male mice (12 weeks old, n = 6 per genotype) were fed on a normal chow diet. Samples were obtained from the femoral artery of awake, freely moving mice. Data are mean ± SEM.
[a] $p < 0.05$ compared to *AceCS2*$^{+/+}$.

After 5 days of LC/HF diet feeding, *AceCS2*$^{-/-}$ mice began to die, and, by 21 days, 50% of the *AceCS2*$^{-/-}$ mice had died. By contrast, none of *AceCS2*$^{+/+}$ mice died (Figure 4G). However, following 21 days on the LC/HF diet, the surviving *AceCS2*$^{-/-}$ mice gradually recovered body temperature and plasma glucose levels. We observed no further excess mortality (data not shown).

Weight, body temperature, and plasma parameters (glucose, NEFA, and ketone bodies) did not differ significantly between the *AceCS2*$^{-/-}$ mice that died and those that survived during the 4 day period of LC/HF feeding after the weaning (Figures S4A–S4E). Therefore, the cause of death was not simply from malnutrition. We also examined the effect of a high-carbohydrate, high-fat (HC/HF) diet (58% fat, 15% protein, and 27% carbohydrate from calories). On this diet, both *AceCS2*$^{-/-}$ and *AceCS2*$^{+/+}$ mice survived with no deaths (data not shown). These data indicated that acetate oxidation mediated by AceCS2 is essential to maintain normal thermogenesis and fuel usage under low-glucose utilization states such as low-carbohydrate diets or fasting.

AceCS2$^{-/-}$ Mice Exhibit Low Body Weight Gain under Low Carbohydrate Intake

We continued to feed the surviving *AceCS2*$^{-/-}$ mice an LC/HF diet. *AceCS2*$^{+/+}$ mice fed on this diet gained weight efficiently; by contrast, *AceCS2*$^{-/-}$ mice exhibited reduced weight gain under this diet (Figure 5A). Food intake was unchanged between

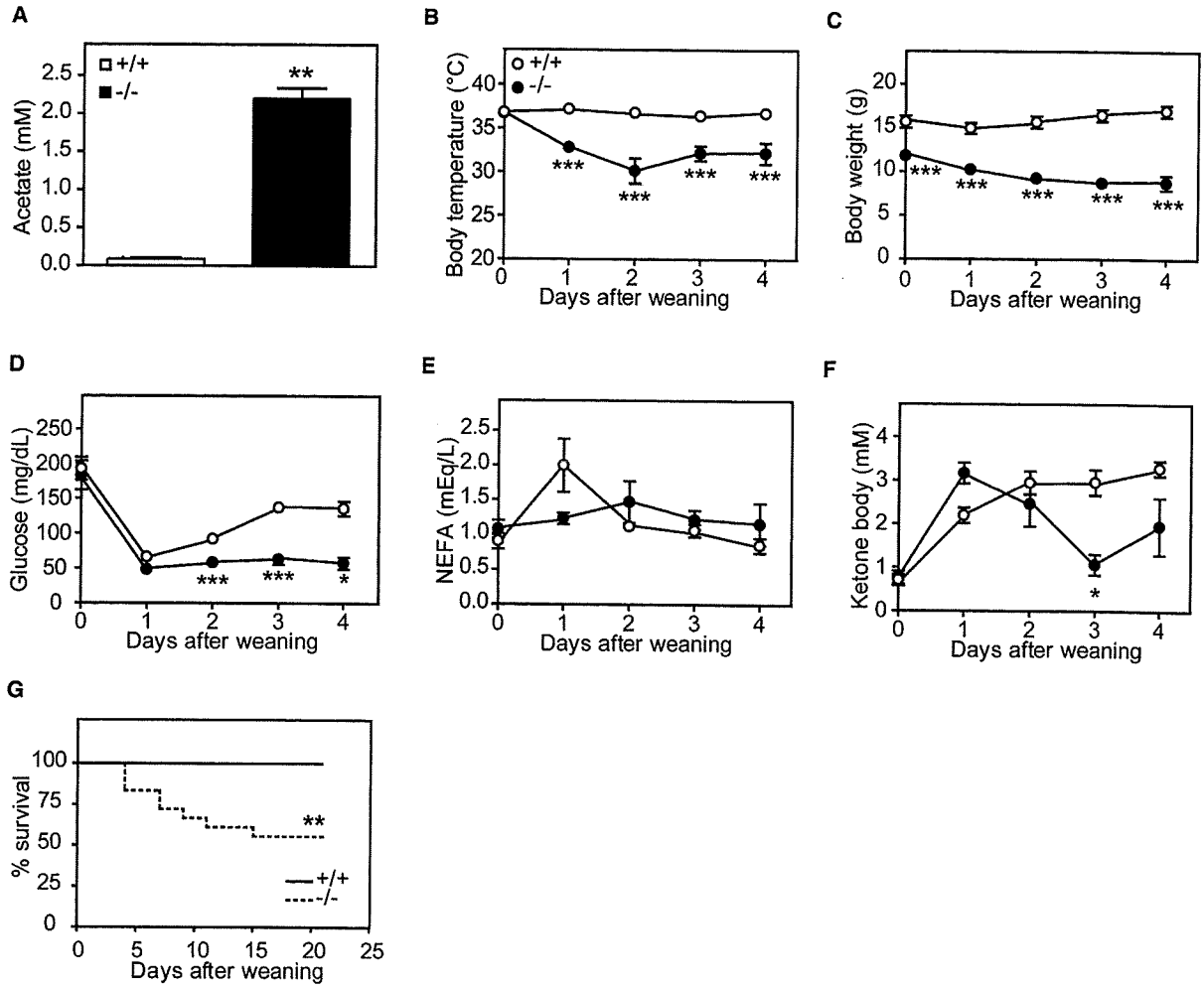

Figure 4. *AceCS2*-Deficient Mice Exhibit Hypothermia When Fed an LC/HF Diet

(A) Male mice (4 weeks old, five per genotype) were fed milk from their mother. Plasma acetate levels were measured.

(B–F) Male mice (4 weeks old) were fed an LC/HF diet. (B) Core rectal temperature, (C) body weight, (D) blood glucose, (E) plasma NEFA, and (F) plasma ketone body level were measured (*AceCS2*$^{+/+}$, n = 8; *AceCS2*$^{-/-}$, n = 7). *p < 0.05, **p < 0.01, and ***p < 0.001 compared to *AceCS2*$^{+/+}$.

(G) Kaplan-Meier analysis of survival in males fed an LC/HF diet at 4 weeks old (*AceCS2*$^{+/+}$, n = 22; *AceCS2*$^{-/-}$, n = 18). **p < 0.001 compared to *AceCS2*$^{+/+}$ by Log-rank test. Data are mean ± SEM.

AceCS2$^{+/+}$ and *AceCS2*$^{-/-}$ mice (Figure 5B). We excised various tissues from these mice and measured tissue weights. The photo shown in Figure 5C was taken for representative mice of each group. There were no marked differences in the weights of liver, kidney, BAT, and heart between *AceCS2*$^{+/+}$ and *AceCS2*$^{-/-}$ mice, but the fat pads of *AceCS2*$^{-/-}$ mice were significantly smaller than those of *AceCS2*$^{+/+}$ mice (Figure 5D). We measured metabolic parameters of these mice at 24 weeks of age (Table 2). Although the plasma glucose levels were unchanged, plasma insulin levels decreased significantly in *AceCS2*$^{-/-}$ mice as compared to *AceCS2*$^{+/+}$ mice. Plasma levels of leptin were 4-fold lower, but plasma acetate was 7-fold higher in *AceCS2*$^{-/-}$ mice (Table 2).

In order to investigate the mechanism underlying reduced weight gain in *AceCS2*$^{-/-}$ mice, food intake and energy expenditure were examined. *AceCS2*$^{-/-}$ mice exhibited consistently higher rates of oxygen consumption and, therefore, had higher metabolic rates than *AceCS2*$^{+/+}$ mice throughout day and night (Figure 5E). After adjusting for allometric scaling and gender, the effect of the *AceCS2*$^{-/-}$ allele was highly significant ($p < 0.01$, n = 7, multiple ANOVA) (Figure 5E, right panel). The respiratory quotient was 0.71 in both *AceCS2*$^{+/+}$ and *AceCS2*$^{-/-}$ mice (data not shown). These data suggested that the resistance to weight gain of *AceCS2*$^{-/-}$ mice may be, at least in part, due to increased energy expenditure. To examine the possibility that fatty acids synthesis is changed in *AceCS2*$^{-/-}$ mice, we measured malonyl-CoA levels and acetyl-CoA carboxylase (ACC) activity (Figure S5). Malonyl-CoA levels and ACC activity in skeletal muscle and BAT did not significantly differ between *AceCS2*$^{-/-}$ and *AceCS2*$^{+/+}$ mice (Figure S5). In liver, malonyl-CoA levels

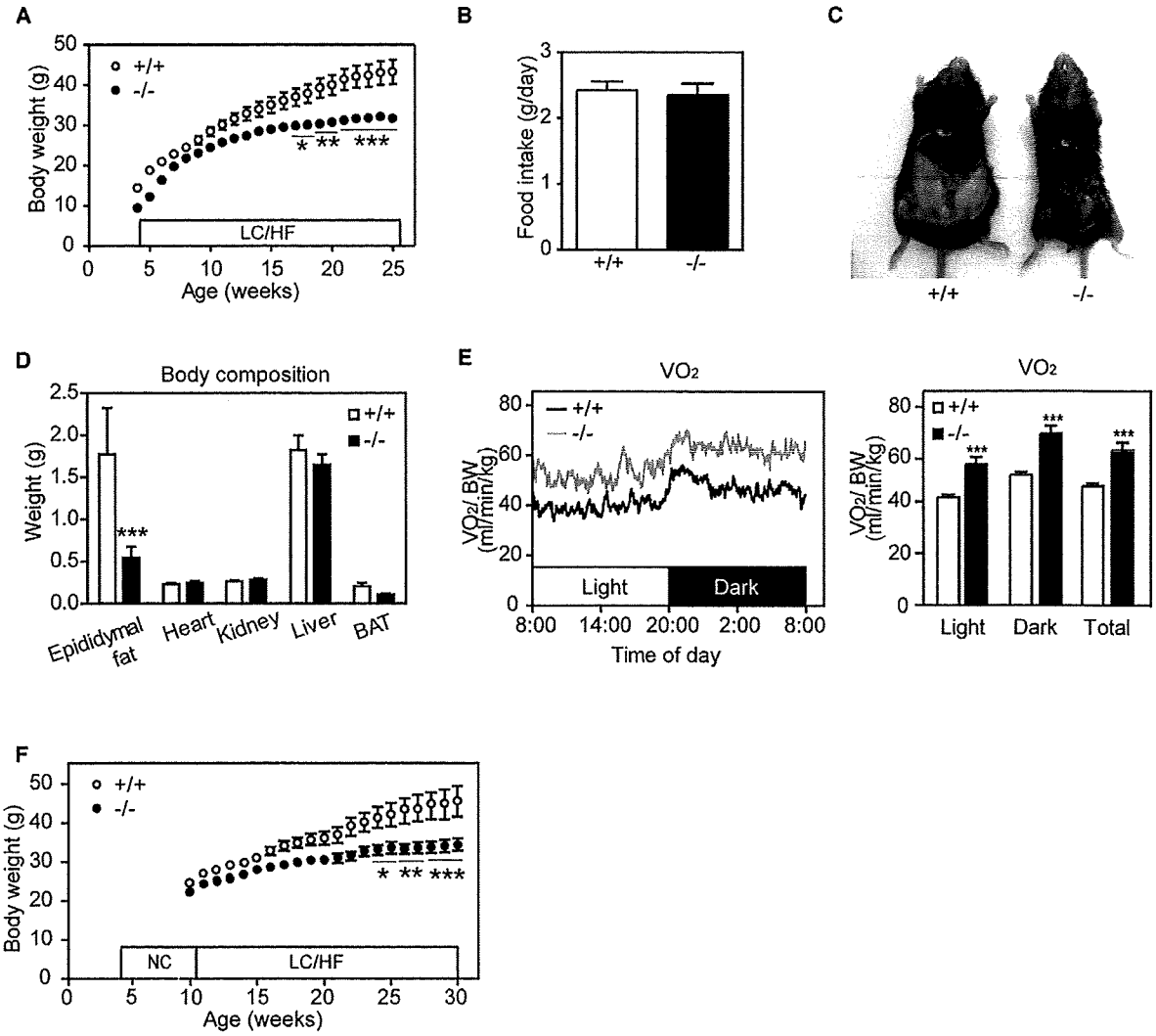

Figure 5. *AceCS2* Deficiency Attenuates Body Weight Gain in Mice Fed an LC/HF Diet

(A) Body weight change of male mice fed an LC/HF diet from 4 weeks old (*AceCS2*$^{+/+}$, n = 15; *AceCS2*$^{-/-}$, n = 12).

(B) Food intake of male mice fed an LC/HF diet at 25 weeks old (*AceCS2*$^{+/+}$, n = 15; *AceCS2*$^{-/-}$, n = 12).

(C) Representative picture of *AceCS2*$^{+/+}$ and *AceCS2*$^{-/-}$ male mice (26 weeks of age) fed an LC/HF diet.

(D) Various tissue weights for *AceCS2*$^{+/+}$ and *AceCS2*$^{-/-}$ male mice (26 weeks of age) fed an LC/HF diet (*AceCS* $^{+/+}$, n = 5; *AceCS2*$^{-/-}$, n = 5).

(E) Oxygen consumption (VO_2, left panel) and average of VO_2 (right panel) were determined in male mice (26 weeks old) fed an LC/HF diet by indirect calorimetry (*AceCS2*$^{+/+}$, n = 8; *AceCS2*$^{-/-}$, n = 7). Data are corrected for body weight. The original, uncorrected data are shown in Figure S6.

(F) Change of body weight. Male mice were weaned at 4 weeks and were fed on normal chow diet for 6 weeks (until 10 weeks of age) and switched to an LC/HF diet (*AceCS2*$^{+/+}$, n = 8; *AceCS2*$^{-/-}$, n = 8). *p < 0.05, **p < 0.01, and ***p < 0.001 compared to *AceCS2*$^{+/+}$. Data are mean ± SEM. NC, normal chow diet.

were reduced by 20% in *AceCS2*$^{-/-}$ (Figure S5), which could be the secondary effect of lower plasma insulin levels since AceCS2 is not expressed in liver. These data suggested that fatty acid synthesis and degradation are not impaired by the deficiency of *AceCS2*.

It is possible that the reduced weight gain of *AceCS2*$^{-/-}$ mice during LC/HF diet feeding simply resulted from a failure to thrive phenotype (reduced body weight gain, hypothermia, hypoglycemia, and low survival rate) induced by low-carbohydrate diet feeding immediately after weaning (Figure 4). Therefore, after weaning, we first fed the mice a normal chow diet for 6 weeks (until 10 weeks of age) and then switched them to an LC/HF diet. By contrast to feeding an LC/HF diet immediately after weaning, none of these *AceCS2*$^{-/-}$ mice died; however, they did exhibit reduced weight gain compared to *AceCS2*$^{+/+}$ mice following the switch to an LC/HF diet (Figure 5F). Reduced weight gain was observed only under a low-carbohydrate regimen. When mice were fed a high-fat, high-carbohydrate diet, *AceCS2*$^{-/-}$ mice were not protected against weight gain (data not shown). These results clearly indicate that adult

Table 2. Metabolic Parameters of *AceCS2*$^{-/-}$ and *AceCS2*$^{+/+}$ Mice Fed an LC/HF Diet

	+/+	−/−
Glucose (mg/dl)	233 ± 14	233 ± 22
Cholesterol (mg/dl)	110 ± 7	70 ± 11[b]
Triglycerides (mg/dl)	93 ± 6	92 ± 9
NEFA (μEql/l)	343 ± 17	332 ± 71
Ketone body (mM)	0.387 ± 0.064	0.705 ± 0.116[a]
Leptin (ng/ml)	2.80 ± 1.12	0.74 ± 1.03[b]
Insulin (ng/ml)	3.34 ± 1.3	1.54 ± 0.71[a]
Acetate (mM)	0.18 ± 0.06	0.97 ± 0.17[b]

Male mice (24 weeks old, seven to nine per genotype) were fed an LC/HF diet. Assays of blood samples were performed on isolated plasma.
[a] $p < 0.05$.
[b] $p < 0.01$ compared to *AceCS2*$^{+/+}$.

AceCS2$^{-/-}$ mice exhibit reduced adiposity under high-fat feeding, low-carbohydrate intake, or ketogenic conditions.

DISCUSSION

Under ketogenic conditions, free fatty acids are released into the circulation and taken up by thermogenic tissues such as BAT and skeletal muscle, where they serve as a fuel for thermogenesis (Picard et al., 2002; Spiegelman and Flier, 2001). Fatty acids are also taken up by liver for the generation of ketone bodies, and these ketone bodies are subsequently utilized in extrahepatic tissues. In addition, previous studies showed that an appreciable amount of acetate is generated in liver and this acetate can subsequently be utilized by extrahepatic tissues (Leighton et al., 1989; Murthy and Steiner, 1973; Seufert et al., 1974). Here, we demonstrate that acetate also serves as a fuel that has specific functions that do not overlap with those of fatty acids and ketone bodies in thermogenesis.

Our studies of mice with targeted deletion of *AceCS2* reveal that these animals can not maintain normal body temperature when starved or when fed an LC/HF diet. Under these conditions, *AceCS2*$^{-/-}$ mice display sustained hypoglycemia, strongly diminished capacity for exercise, and dramatically increased mortality as compared to their wild-type or heterozygous littermates. The mutant animals also exhibit strikingly reduced rates of whole-body acetate oxidation and correspondingly increased levels of acetate in plasma. Most importantly, ATP levels in the skeletal muscle of 48 hr fasted *AceCS2*$^{-/-}$ mice were profoundly reduced, showing the significant contribution of acetate and AceCS2 to the energy supply under ketogenic conditions. Therefore, under ketogenic conditions, the hypothermia and poor exercise tolerance observed in the *AceCS2*$^{-/-}$ mice is most likely from a lack of acetate utilization as a fuel source. Supporting this possibility, plasma acetate levels were significantly higher under fasting conditions than under fed conditions. This suggests that acetate turnover is significantly higher in the fasted state primarily due to AceCS2.

LC/HF diet has been generally recognized to have weight-reducing effects on obese animals (Kennedy et al., 2007). Although the body weight gain of mice fed an LC/HF diet is significantly lower than that of those fed high-fat and high-carbohydrate diets, our LC/HF diet has no weight-reducing or anti-weight-gaining effect. In the experiments done by Kennedy et al. (2007), 8-week-old mice fed a normal chow diet were switched to an LC/HF diet, and the weight of mice fed an LC/HF diet dropped until it stabilized at 85% of the initial weight. The discrepancy between these results may result from the difference in the composition of the different LC/HF diets. The LC/HF diet that Kennedy et al. used consists of 78.85% fat, 9.5% protein, and 0.76% carbohydrate, whereas our LC/HF diet (purchased from Harlan Teklad) contains 67.4% fat, 15.3% protein, and 0.6% carbohydrate (% by weight). In addition, the source of the fat is also different. The LC/HF diet in their study contains lard and butter, whereas our LC/HF diet contains vegetable shortening. Regardless of the differences in the exact diet, we show that AceCS2 is critical for normal body weight gain under an LC/HF diet.

Recent observations indirectly support a role for *AceCS2* as a determinant of growth and adiposity. From the mapping of a quantitative trait locus (QTL) region on mouse chromosome 2 that has a large effect on growth and adiposity, AceCS2 was reported as 1 of 18 candidate genes potentially controlling predisposition to growth and predisposition to obesity (Jerez-Timaure et al., 2005).

Although plasma acetate is very high in *AceCS2*$^{-/-}$ mice, we found that there was appropriate and sufficient respiratory compensation for any metabolic acidosis caused by acetate accumulation. *AceCS2*$^{-/-}$ mice exhibited hypocapnea to maintain a neutral arterial blood pH. Patients with chronic obstructive lung disease and cystic fibrosis commonly have low body weight, which is believed to be related to inadequate energy intake, nutrient malabsorption, and excessive energy expenditure (Bell et al., 1996). Basal metabolic rate is 10%–20% greater in these patients than in healthy subjects and may contribute to their energy imbalance. Furthermore, increased oxygen consumption caused by increased respiratory muscle activity has been reported in these patients, which largely explains the increased basal metabolic rate (Campbell et al., 1959; Cherniack, 1959; Donahoe et al., 1989; McGregor and Becklake, 1961). Because *AceCS2*$^{-/-}$ mice seem to be hyperventilating, this increased use of respiratory muscles might account for, at least in part, the higher oxygen consumption.

We previously identified AceCS2 as a target of KLF15 (Yamamoto et al., 2004). The fasting-induced transcription of AceCS2 is largely dependent on KLF15. Similarly to *AceCS2*$^{-/-}$ mice, KLF15-deficient mice also exhibit severe hypoglycemia after overnight fasting (Fisch et al., 2007). KLF15 plays an important role in gluconeogenesis by regulating amino acid degradation and key gluconeogenic enzymes such as phosphoenolpyruvate carboxykinase in the liver during fasting (Gray et al., 2007; Teshigawara et al., 2005). Our data indicate that KLF15 is crucial for survival during starvation through two mechanisms: (1) gluconeogenesis in liver and (2) acetate oxidation to generate ATP and heat in muscle and BAT through AceCS2 activity.

The sirtuins comprise a conserved family of proteins that are believed to mediate some of the health benefits of calorie restriction, which leads to extension of life span in nearly all organisms studied, including mammals. SIRT1 has been reported to function as an energy-sensing gene that senses NAD^+ levels and regulates the activity of critical transcriptional regulators of

metabolism in multiple tissues (Yang et al., 2007). Within the mitochondria, SIRT3 deacetylates a key lysine residue on AceCS2, leading to its enzymatic activation (Hallows et al., 2006; Schwer et al., 2006; Schwer and Verdin, 2008). As SIRT3 protein levels are specifically increased in calorie-restricted mammals, regulation of AceCS2 activity by SIRT3 could be a key metabolic factor responsible for homeostatic regulation during calorie restriction, leading to its positive effect on life span. Sirt3 was recently shown to be necessary for maintaining basal ATP levels with ATP levels in multiple organs of *Sirt3*$^{-/-}$ mice that are markedly reduced compared to wild-type levels (Ahn et al., 2008). This study, along with ours, suggests that activation of AceCS2 by Sirt3 is required to maintain basal ATP levels in mammals. Future studies of AceCS2- and AceCS2-deficient mice are warranted to investigate this potentially exciting link between longevity and mitochondrial energy metabolism.

In conclusion, our current findings demonstrate that acetate metabolism mediated by AceCS2 is crucial for survival and energy production under ketogenic conditions such as starvation or diabetes. These and future studies of acetate metabolism mediated by AceCS2 will have a significant impact on the understanding of the acetate metabolism for heat generation and energy metabolism.

EXPERIMENTAL PROCEDURES

Generation of AceCS2-Deficient Mice

We constructed a targeting plasmid by using genomic DNA fragments derived from Sv129 mice. A Lac Z and a neomycin cassette flanked by two loxP sites were introduced into the *AceCS2* locus of ES cells (derived from the Sv129 strain). Electroporation, selection, and screening were performed with standard gene-targeting techniques. Briefly, genomic DNA was isolated from neomycin-resistant ES cell clones, digested with KpnI, and subjected to hybridization with a probe to detect homologous recombination and the presence of the flox allele (Figure 1A).

Chimeric males were generated by using the morula aggregation technique and mated to C57BL/6J female mice. Homologous recombination was confirmed by Southern blotting (Figure 1B). Deletion of RNA transcripts and protein was confirmed by QRT-PCR and western blotting, respectively (Figures 1D and 1E). After achieving germline transmission, *AceCS2*$^{+/-}$ mice were crossed with C57BL/6J for six to nine generations.

Heterozygous mice were mated to obtain *AceCS2*$^{-/-}$ mice. Wild-type littermates were used as controls throughout the study. Genotyping of mice used in this study was performed by PCR of tail DNA as shown in Figure 1C; the mutant allele was detected by using a pair of oligonucleotides (5′-GGCGCACAA CAAAACCTAGT-3′ and 5′-GACAGTATCGGCCTCAGGAA-3′) that amplify a 512 bp PCR product between the *AceCS2* and sequence 3′ to *Lac Z/neo* cassette. The wild-type allele was detected by PCR with a pair of oligonucleotides (5′-GGCGCACAACAAAACCTAGT-3′ and 5′-GGGGTTCGTGCCTGGTTG-3′) that amplify a 355 bp PCR product spanning exon 1.

Quantitative Real-Time PCR

Quantitative real-time PCR (QRT-PCR) was performed as previously described (Tanaka et al., 2003). All primer sequences used in this paper are available upon request.

Antibody

To produce rabbit polyclonal anti-murine AceCS2 (IgGA001), a 12-residue peptide corresponding to the C terminus of murine AceCS2 (CQKYEEQ RAATN) was synthesized (Sigma Genesis, Japan), coupled to keyhole limpet hemocyanin, and injected into New Zealand White rabbits. IgG fractions were prepared by affinity chromatography on protein A-Sepharose (GE Healthcare Bioscience). For immunoblot analysis, an aliquot of whole-cell lysates from heart (20 μg) was subjected to SDS-PAGE on 10% gels followed by analysis with a 1:1000 dilution of anti-AceCS2 (Fujino et al., 2001).

Animal Experiments

All procedures were performed in accordance with Japanese Physiological Society guidelines for animal care. Mice were group housed in cages with a 12 hr light/12 hr dark cycle and fed a standard rodent chow diet (CE-2; CLEA Japan, Osaka). To induce a ketogenic condition, we compared an LC/HF diet (Table S3; Rho et al., 1999) (TD96355; Harlan Teklad Premier Laboratory Diets) consisting of 90.5% fat, 9.1% protein, and 0.4% carbohydrate (0% sucrose from calories) to a high-carbohydrate, high-fat diet consisting of 58.0% fat, 15.0% protein, and 27.01% carbohydrate from calories (Tanaka et al., 2003). All mice had free access to water. Food consumption was monitored daily, and body weight was recorded every week, unless otherwise stated.

Core body temperature was monitored using a rectal thermometer at 10 a.m. For the exercise performance, the mice were trained on the treadmill (MK-680AT/02M, Muromachikikai, Tokyo) prior to the exercise performance test (a 10 min run at 10 m/min at a 5° incline once per day for 4 days). Exhaustion was defined as the point at which mice were unable to continue running.

Food Intake, Locomotor Activity, and Metabolic Rate Measurement

Male mice (26 weeks old) were housed under controlled lighting (12 hr light-dark cycle) and temperature (23°C) conditions. Food (standard chow pellets or an LC/HF diet) and water were available ad libitum. Mice were then housed singly under the same conditions as above for an acclimation period of at least 7 days. Body weights and food intake were monitored daily for the duration of the study. Energy expenditure was measured by indirect calorimetry as described previously (MK-5000RQ; Muromachi, Tokyo) (Takayasu et al., 2006). Mice were placed in the calorimeter chambers and acclimated for 1 day. Locomotor activity was measured by using an infrared (IR) passive sensor system as described previously (Supermex, Muromachi Kikai, Japan) (Takayasu et al., 2006). The experiment was started at 8 a.m. (light period).

Acetate Oxidation

Acetate ([1-^{14}C]acetate, CFA13, GE Healthcare UK Limited) oxidation was measured in vivo as described (Wolfgang et al., 2006). The in vivo rate of ^{14}C-acetate oxidation (2 μCi [1 Ci = 37 GBq] of [1-^{14}C]acetate injected intraperitoneally) to $^{14}CO_2$ was determined after treatment of mice. Mice were acclimated in metabolic chambers fitted with 2-aminoethanol traps to recover expired $^{14}CO_2$. The oxidation of [1-^{14}C]acetate to form $^{14}CO_2$ was measured at 20 min intervals over the next 1 hr. At the end of experiment, plasma was collected, and plasma [1-^{14}C]acetate was measured.

Acetate Measurement

Plasma acetate levels were measured as described by (Hillman et al. 1978) with slight modifications. Briefly, plasma was mixed with 1 mM isovaleric acid as the internal standard. The sample was acidified with one-fifth the volume of 10% sulfosalicylic acid and then extracted three times with 10 volumes of diethylether. The ether extract was immediately back extracted into 0.2 M NaOH. The ether was removed under a stream of dry nitrogen. Before injection, the sample was reacidified with one-fifth the volume of 10% phosphoric acid. The acetate concentration of the sample was analyzed by gas chromatograph (GC-2014, Shimadzu, Japan) equipped with a flame ionization detector and a capillary column (ULBON HR-20 M, 0.25 mm i.d. × 25 m × 0.25 μm). The column was operated at 140°C. The injection port and the flame ionization detector were maintained at 300°C. The chromatograph was standardized with a mixture of C2-C7 short-chain fatty acids.

Plasma Parameters

Mice were sacrificed by CO_2 asphyxiation following a 4 hr fast during the light cycle (food removed 9:00 a.m., sacrificed at 1:00 p.m.). Blood was drawn by cardiac puncture, and the plasma was separated immediately by centrifugation and stored at −80°C until use. Plasma glucose, NEFA, triglycerides, total cholesterol, and total ketone body levels were determined by Glucose C2-test (Wako Pure Chemical, Japan), NEFA C-test (Wako Pure Chemical, Japan), Triglyceride E-test (Wako Pure Chemical, Japan), Cholesterol E-test (Wako Pure Chemical, Japan), and Autokit Total Ketone Bodies (Wako Pure

Chemical, Japan), respectively. Plasma insulin and leptin levels were determined by ELISA with an insulin immunoassay kit (Shibayagi, Japan) and a mouse leptin immunoassay (R & D systems) according to the manufacturer's instructions.

Assay Procedure for Acetyl-CoA, Adenine Nucleotides, NAD^+, and NADH Contents

Acetyl-CoA and adenine nucleotide contents in skeletal muscle or BAT of 12-week-old male mice were measured essentially as described previously (Miura et al., 2006; Scott et al., 1992; Takamura et al., 1985). NAD^+ and NADH nucleotide concentrations were directly measured by NAD^+/NADH Assay kit (Biochain Institute, Inc.) according to the manufacturer's instructions. The detail methods are described in the Supplemental Experimental Procedures.

Blood Gas Analysis

Blood gas analysis was performed as previously described (Kuwaki et al., 1996). A catheter was implanted into the right femoral artery under isoflurane (2%–3%) anesthesia. Up to 70 μl of arterial blood was drawn from the indwelling catheter after a recovery period of more than 2 hr and when the animal was quietly awake. Blood gases were determined by a blood gas analyzer (ABL500, Radiometer, Copenhagen).

Statistical Analyses

All values are expressed as mean ± standard error of the mean unless otherwise specified. Significant differences between mean values were evaluated using two-tailed, unpaired Student's t test (when two groups were analyzed) or one-way ANOVA followed by Student Newman-Keuls test (for three or more groups).

SUPPLEMENTAL DATA

Supplemental Data include Supplemental Experimental Procedures, six figures, and three tables and can be found with this article online at: http://www.cell.com/cell-metabolism/supplemental/S1550-4131(08)00393-8.

ACKNOWLEDGMENTS

We thank Dr. Rob Rawson for critical reading of the manuscript; Drs. Peter Edwards and Mitsuhiro Watanabe for helpful discussions; and Kaori Ikeda, Junko Kuno, Satomi Takahashi, Yuko Kai, and Mika Nomiyama for technical assistance. This work was supported through ERATO JST, NIBIO by the NFAT project of the NEDO and by the Special Coordination Fund for Science and Technology from the Ministry of Education, Culture, Sports, Science, and Technology. This work was also supported, in part, by Astellas Foundation for Research on Metabolic Disorders, the Uehara Memorial Foundation, and the Ono Medical Foundation. M.Y. is an Investigator of the Howard Hughes Medical Institute. J.S. is an Investigator of Translational Systems Biology and Medicine Initiative (TSBMI).

Received: June 6, 2008
Revised: October 15, 2008
Accepted: December 12, 2008
Published: February 3, 2009

REFERENCES

Ahn, B.H., Kim, H.S., Song, S., Lee, I.H., Liu, J., Vassilopoulos, A., Deng, C.X., and Finkel, T. (2008). A role for the mitochondrial deacetylase Sirt3 in regulating energy homeostasis. Proc. Natl. Acad. Sci. USA *105*, 14447–14452.

Bell, S.C., Saunders, M.J., Elborn, J.S., and Shale, D.J. (1996). Resting energy expenditure and oxygen cost of breathing in patients with cystic fibrosis. Thorax *51*, 126–131.

Campbell, E.J., Westlake, E.K., and Cherniack, R.M. (1959). The oxygen consumption and efficiency of the respiratory muscles of young male subjects. Clin. Sci. (Lond.) *18*, 55–64.

Cherniack, R.M. (1959). The oxygen consumption and efficiency of the respiratory muscles in health and emphysema. J. Clin. Invest. *38*, 494–499.

Donahoe, M., Rogers, R.M., Wilson, D.O., and Pennock, B.E. (1989). Oxygen consumption of the respiratory muscles in normal and in malnourished patients with chronic obstructive pulmonary disease. Am. Rev. Respir. Dis. *140*, 385–391.

Fisch, S., Gray, S., Heymans, S., Haldar, S.M., Wang, B., Pfister, O., Cui, L., Kumar, A., Lin, Z., Sen-Banerjee, S., et al. (2007). Kruppel-like factor 15 is a regulator of cardiomyocyte hypertrophy. Proc. Natl. Acad. Sci. USA *104*, 7074–7079.

Fujino, T., Kondo, J., Ishikawa, M., Morikawa, K., and Yamamoto, T.T. (2001). Acetyl-CoA synthetase 2, a mitochondrial matrix enzyme involved in the oxidation of acetate. J. Biol. Chem. *276*, 11420–11426.

Fukao, T., Lopaschuk, G.D., and Mitchell, G.A. (2004). Pathways and control of ketone body metabolism: On the fringe of lipid biochemistry. Prostaglandins Leukot. Essent. Fatty Acids *70*, 243–251.

Gray, S., Wang, B., Orihuela, Y., Hong, E.G., Fisch, S., Haldar, S., Cline, G.W., Kim, J.K., Peroni, O.D., Kahn, B.B., et al. (2007). Regulation of gluconeogenesis by Kruppel-like factor 15. Cell Metab. *5*, 305–312.

Hallows, W.C., Lee, S., and Denu, J.M. (2006). Sirtuins deacetylate and activate mammalian acetyl-CoA synthetases. Proc. Natl. Acad. Sci. USA *103*, 10230–10235.

Hillman, R.E. (1978). Simple, rapid method for determination of propionic acid and other short-chain fatty acids in serum. Clin. Chem. *24*, 800–803.

Ikeda, Y., Yamamoto, J., Okamura, M., Fujino, T., Takahashi, S., Takeuchi, K., Osborne, T.F., Yamamoto, T.T., Ito, S., and Sakai, J. (2001). Transcriptional regulation of the murine acetyl-CoA synthetase 1 gene through multiple clustered binding sites for sterol regulatory element-binding proteins and a single neighboring site for Sp1. J. Biol. Chem. *276*, 34259–34269.

Jerez-Timaure, N.C., Eisen, E.J., and Pomp, D. (2005). Fine mapping of a QTL region with large effects on growth and fatness on mouse chromosome 2. Physiol. Genomics *21*, 411–422.

Kennedy, A.R., Pissios, P., Otu, H., Xue, B., Asakura, K., Furukawa, N., Marino, F.E., Liu, F.F., Kahn, B.B., Libermann, T.A., et al. (2007). A high-fat, ketogenic diet induces a unique metabolic state in mice. Am. J. Physiol. Endocrinol. Metab. *292*, E1724–E1739.

Kuwaki, T., Cao, W.H., Kurihara, Y., Kurihara, H., Ling, G.Y., Onodera, M., Ju, K.H., Yazaki, Y., and Kumada, M. (1996). Impaired ventilatory responses to hypoxia and hypercapnia in mutant mice deficient in endothelin-1. Am. J. Physiol. *270*, R1279–R1286.

Leighton, F., Bergseth, S., Rortveit, T., Christiansen, E.N., and Bremer, J. (1989). Free acetate production by rat hepatocytes during peroxisomal fatty acid and dicarboxylic acid oxidation. J. Biol. Chem. *264*, 10347–10350.

Lowell, B.B., and Spiegelman, B.M. (2000). Towards a molecular understanding of adaptive thermogenesis. Nature *404*, 652–660.

Luong, A., Hannah, V.C., Brown, M.S., and Goldstein, J.L. (2000). Molecular characterization of human acetyl-CoA synthetase, an enzyme regulated by sterol regulatory element-binding proteins. J. Biol. Chem. *275*, 26458–26466.

Matthias, A., Ohlson, K.B., Fredriksson, J.M., Jacobsson, A., Nedergaard, J., and Cannon, B. (2000). Thermogenic responses in brown fat cells are fully UCP1-dependent. UCP2 or UCP3 do not substitute for UCP1 in adrenergically or fatty scid-induced thermogenesis. J. Biol. Chem. *275*, 25073–25081.

McGregor, M., and Becklake, M.R. (1961). The relationship of oxygen cost of breathing to respiratory mechanical work and respiratory force. J. Clin. Invest. *40*, 971–980.

Miura, S., Tomitsuka, E., Kamei, Y., Yamazaki, T., Kai, Y., Tamura, M., Kita, K., Nishino, I., and Ezaki, O. (2006). Overexpression of peroxisome proliferator-activated receptor gamma co-activator-1alpha leads to muscle atrophy with depletion of ATP. Am. J. Pathol. *169*, 1129–1139.

Murthy, V.K., and Steiner, G. (1973). Hepatic acetate levels in relation to altered lipid metabolism. Metabolism *22*, 81–84.

Picard, F., Gehin, M., Annicotte, J., Rocchi, S., Champy, M.F., O'Malley, B.W., Chambon, P., and Auwerx, J. (2002). SRC-1 and TIF2 control energy balance between white and brown adipose tissues. Cell *111*, 931–941.

Rho, J.M., Kim, D.W., Robbins, C.A., Anderson, G.D., and Schwartzkroin, P.A. (1999). Age-dependent differences in flurothyl seizure sensitivity in mice treated with a ketogenic diet. Epilepsy Res. *37*, 233–240.

Schwer, B., Bunkenborg, J., Verdin, R.O., Andersen, J.S., and Verdin, E. (2006). Reversible lysine acetylation controls the activity of the mitochondrial enzyme acetyl-CoA synthetase 2. Proc. Natl. Acad. Sci. USA *103*, 10224–10229.

Schwer, B., and Verdin, E. (2008). Conserved metabolic regulatory functions of sirtuins. Cell Metab. *7*, 104–112.

Scott, M.D., Baudendistel, L.J., and Dahms, T.E. (1992). Rapid separation of creatine, phosphocreatine and adenosine metabolites by ion-pair reversed-phase high-performance liquid chromatography in plasma and cardiac tissue. J. Chromatogr. *576*, 149–154.

Seufert, C.D., Graf, M., Janson, G., Kuhn, A., and Soling, H.D. (1974). Formation of free acetate by isolated perfused livers from normal, starved and diabetic rats. Biochem. Biophys. Res. Commun. *57*, 901–909.

Spiegelman, B.M., and Flier, J.S. (2001). Obesity and the regulation of energy balance. Cell *104*, 531–543.

Takamura, Y., Kitayama, Y., Arakawa, A., Yamanaka, S., Tosaki, M., and Ogawa, Y. (1985). Malonyl-CoA: Acetyl-CoA cycling. A new micromethod for determination of acyl-CoAs with malonate decarboxylase. Biochim. Biophys. Acta *834*, 1–7.

Takayasu, S., Sakurai, T., Iwasaki, S., Teranishi, H., Yamanaka, A., Williams, S.C., Iguchi, H., Kawasawa, Y.I., Ikeda, Y., Sakakibara, I., et al. (2006). A neuropeptide ligand of the G protein-coupled receptor GPR103 regulates feeding, behavioral arousal, and blood pressure in mice. Proc. Natl. Acad. Sci. USA *103*, 7438–7443.

Tanaka, T., Yamamoto, J., Iwasaki, S., Asaba, H., Hamura, H., Ikeda, Y., Watanabe, M., Magoori, K., Ioka, R.X., Tachibana, K., et al. (2003). Activation of peroxisome proliferator-activated receptor delta induces fatty acid beta-oxidation in skeletal muscle and attenuates metabolic syndrome. Proc. Natl. Acad. Sci. USA *100*, 15924–15929.

Teshigawara, K., Ogawa, W., Mori, T., Matsuki, Y., Watanabe, E., Hiramatsu, R., Inoue, H., Miyake, K., Sakaue, H., and Kasuga, M. (2005). Role of Kruppel-like factor 15 in PEPCK gene expression in the liver. Biochem. Biophys. Res. Commun. *327*, 920–926.

Wolfgang, M.J., Kurama, T., Dai, Y., Suwa, A., Asaumi, M., Matsumoto, S., Cha, S.H., Shimokawa, T., and Lane, M.D. (2006). The brain-specific carnitine palmitoyltransferase-1c regulates energy homeostasis. Proc. Natl. Acad. Sci. USA *103*, 7282–7287.

Yamamoto, J., Ikeda, Y., Iguchi, H., Fujino, T., Tanaka, T., Asaba, H., Iwasaki, S., Ioka, R.X., Kaneko, I.W., Magoori, K., et al. (2004). A Kruppel-like factor KLF15 contributes fasting-induced transcriptional activation of mitochondrial acetyl-CoA synthetase gene AceCS2. J. Biol. Chem. *279*, 16954–16962.

Yamashita, H., Kaneyuki, T., and Tagawa, K. (2001). Production of acetate in the liver and its utilization in peripheral tissues. Biochim. Biophys. Acta *1532*, 79–87.

Yang, H., Yang, T., Baur, J.A., Perez, E., Matsui, T., Carmona, J.J., Lamming, D.W., Souza-Pinto, N.C., Bohr, V.A., Rosenzweig, A., et al. (2007). Nutrient-sensitive mitochondrial NAD+ levels dictate cell survival. Cell *130*, 1095–1107.

THE JOURNAL OF BIOLOGICAL CHEMISTRY VOL. 284, NO. 11, pp. 7255–7263, March 13, 2009

Novel Mitochondrial Complex II Isolated from *Trypanosoma cruzi* Is Composed of 12 Peptides Including a Heterodimeric Ip Subunit*[S]

Received for publication, August 26, 2008, and in revised form, January 2, 2009 Published, JBC Papers in Press, January 2, 2009, DOI 10.1074/jbc.M806623200

Jorge Morales[‡1], Tatsushi Mogi[‡2], Shigeru Mineki[§], Eizo Takashima[‡3], Reiko Mineki[¶], Hiroko Hirawake[‡], Kimitoshi Sakamoto[‡], Satoshi Ōmura[‖], and Kiyoshi Kita[‡4]

From the [‡]Department of Biomedical Chemistry, Graduate School of Medicine, the University of Tokyo, Hongo, Bunkyo-ku, Tokyo 113-0033, the [§]Department of Applied Biological Science, Faculty of Science and Technology, Tokyo University of Science, Noda, Chiba 278-8510, the [¶]Division of Proteomics and BioMolecular Science, Juntendo University Graduate School of Medicine, Hongo, Bunkyo-ku, Tokyo 113-8421, and the [‖]Kitasato Institute for Life Sciences and Graduate School of Infection Control Sciences, Kitasato University, Minato-ku, Tokyo 108-8641, Japan

Mitochondrial respiratory enzymes play a central role in energy production in aerobic organisms. They differentiated from the α-proteobacteria-derived ancestors by adding non-catalytic subunits. An exception is Complex II (succinate: ubiquinone reductase), which is composed of four α-proteobacteria-derived catalytic subunits (SDH1–SDH4). Complex II often plays a pivotal role in adaptation of parasites in host organisms and would be a potential target for new drugs. We purified Complex II from the parasitic protist *Trypanosoma cruzi* and obtained the unexpected result that it consists of six hydrophilic (SDH1, $SDH2_N$, $SDH2_C$, and SDH5–SDH7) and six hydrophobic (SDH3, SDH4, and SDH8–SDH11) nucleus-encoded subunits. Orthologous genes for each subunit were identified in *Trypanosoma brucei* and *Leishmania major*. Notably, the iron-sulfur subunit was heterodimeric; $SDH2_N$ and $SDH2_C$ contain the plant-type ferredoxin domain in the N-terminal half and the bacterial ferredoxin domain in the C-terminal half, respectively. Catalytic subunits (SDH1, $SDH2_N$ plus $SDH2_C$, SDH3, and SDH4) contain all key residues for binding of dicarboxylates and quinones, but the enzyme showed the lower affinity for both substrates and inhibitors than mammalian enzymes. In addition, the enzyme binds protoheme IX, but SDH3 lacks a ligand histidine. These unusual features are unique in the Trypanosomatida and make their Complex II a target for new chemotherapeutic agents.

The parasitic protist *Trypanosoma cruzi* is the etiological agent of Chagas disease, a public health threat in Central and South America. These parasites are normally transmitted by reduviid bugs via the vector feces after a bug bite and also via transfusion of infected blood. About 16–18 million people are infected, and 100 million are at risk, but there are no definitive chemotherapeutic treatments available (1). Despite having potential pathways for oxidative phosphorylation (2), all trypanosomatids (*Trypanosoma* and *Leishmania* species) analyzed so far are characterized by incomplete oxidation of glucose with secretion of end products, such as succinate, alanine, ethanol, acetate, pyruvate, and glycerol (3, 4) (Fig. 1). Major routes for formation of succinate in *Trypanosoma brucei* are via NADH-dependent fumarate reductase in glycosomes and mitochondria (5, 6). In trypanosomatid mitochondria, the Krebs cycle is inefficient, and pyruvate is principally converted to acetate via acetate:succinate CoA transferase (7). A part of the Krebs cycle operates the utilization of histidine in the insect stage of *T. cruzi* (8).

Mitochondrial Complex II (succinate:quinone reductase (SQR)[5] and succinate dehydrogenase (SDH)) serves as a membrane-bound Krebs cycle enzyme and often plays a pivotal role in adaptation of parasites to environments in their host (9, 10). In general, Complex II consists of four subunits (11). A flavoprotein subunit (SDH1, Fp) and an iron-sulfur subunit (SDH2, Ip) form a soluble heterodimer, which then binds to a membrane anchor heterodimer, SDH3 (CybL) and SDH4 (CybS). SDH1 contains a covalently bound FAD and catalyzes the oxidation of succinate to fumarate. SDH2 transfers electrons to ubiquinone via the [2Fe-2S] cluster in the N-terminal plant-type ferredoxin domain (Ip_N) and the [4Fe-4S] and [3Fe-4S] clusters in the C-terminal bacterial ferredoxin domain (Ip_C). Ubiquinone is bound and reduced in a pocket provided by SDH2, SDH3, and SDH4 (12–14). SDH3 and SDH4 contain three transmembrane helices and coordinate protoheme IX via histidine in the second helices of each subunit (11–14).

* This work was supported in part by Grant-in-aid for Scientific Research 20570124 (to T. M.), Creative Scientific Research Grant 18GS0314 (to K. K.), Grant-in-aid for Scientific Research on Priority Areas 18073004 (to K. K.) from the Japanese Society for the Promotion of Science, and Targeted Proteins Research Program (to K. K.) from the Japanese Ministry of Education, Science, Culture, Sports and Technology (MEXT). The costs of publication of this article were defrayed in part by the payment of page charges. This article must therefore be hereby marked "*advertisement*" in accordance with 18 U.S.C. Section 1734 solely to indicate this fact.

[S] The on-line version of this article (available at http://www.jbc.org) contains supplemental Table S1.

[1] Supported by a Japanese Government scholarship from Ministry of Education, Science, Culture, Sports and Technology.

[2] To whom correspondence may be addressed. Tel.: 81-3-5841-3526; Fax: 81-3-5841-3444; E-mail: tmogi@m.u-tokyo.ac.jp.

[3] Present address: Dept. of Microbiology, School of Life Dentistry at Tokyo, Nippon Dental University, Tokyo 102-8159, Japan.

[4] To whom correspondence may be addressed. Tel.: 81-3-5841-3526; Fax: 81-3-5841-3444; E-mail: kitak@m.u-tokyo.ac.jp.

[5] The abbreviations used are: SQR, succinate:quinone reductase; hrCNE, high resolution clear native electrophoresis; IC_{50}, the 50% inhibitory concentration; Ip_N, the N-terminal plant-type ferredoxin domain; Ip_C, the C-terminal bacterial ferredoxin domain; DCIP, 2,4-dichlorophenolindophenol; SML, sucrose monolaurate; Tricine, *N*-[2-hydroxy-1,1-bis(hydroxymethyl)ethyl]-glycine; MOPS, 3-(*N*-morpholino)propanesulfonic acid; Q_n, ubiquinone-*n*.

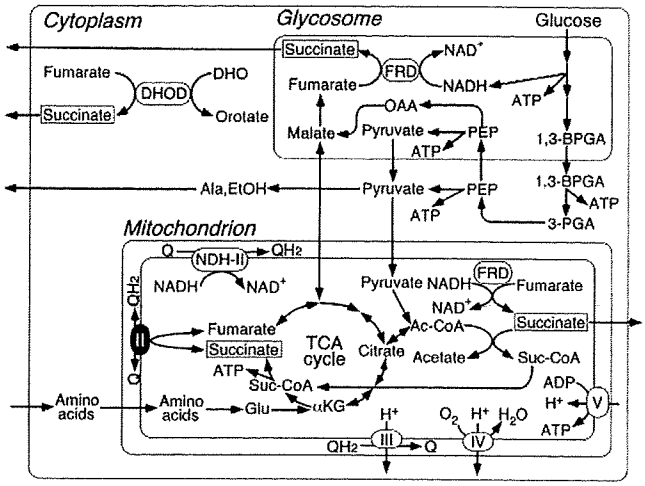

FIGURE 1. **Metabolic pathways in *T. cruzi*.** Incomplete oxidation of glucose takes place in glycosomes and mitochondria, and end products such as succinate, L-alanine, ethanol, and acetate are excreted from parasites (3, 4). Cytoplasmic dihydroorotate (*DHO*):fumarate reductase (*DHOD*) contributes succinate production (6).

Parasitic nematodes adapted to hypoxic host environments often have modified respiratory chains. Many adult parasites perform fumarate respiration by expressing a stage-specific isoform of Complex II (9, 10). *Hemonchus contortus* uses an isoform for SDH2 (9), whereas *Ascaris suum* uses isoforms for SDH1 and SDH4 (10). To explore the adaptive strategy in a parasitic protist, we isolated mitochondria from axenic culture of *T. cruzi* epimastigotes and characterized the purified Complex II. Our results demonstrated for the first time that *T. cruzi* Complex II is an unusual supramolecular complex with a heterodimeric iron-sulfur subunit and seven novel noncatalytic subunits. Purified enzyme showed reduced binding affinities for both substrates and inhibitors. Because this novel structural organization is conserved in all trypanosomatids (2, 15, 16), parasite Complex II would be a potential target for the development of new chemotherapeutic agents for trypanosomiasis and leishmaniasis.

EXPERIMENTAL PROCEDURES

Preparation of Mitochondria—T. cruzi strain Tulahuhen was grown statically for 6–7 days at 26 °C in 300-cm^2 cell culture flasks (Falcon, BD Biosciences) containing 250 ml of the modified LIT medium (17), supplemented with 0.1% (w/v) glucose, 0.001% (w/v) hemin (Sigma), and 5% (v/v) fetal bovine serum (MP Biochemicals). Mitochondria were isolated from epimastigotes by the differential centrifugation method (18) with slight modifications. Parasites grown to $6-8 \times 10^7$ cells/ml were washed with buffer A (20 mM Tris-HCl, pH 7.2, 10 mM NaH_2PO_4, 1 mM sodium EDTA, 1 mM dithiothreitol, 0.225 M sucrose, 20 mM KCl, and 5 mM $MgCl_2$). Cells were disrupted by grinding with silicon carbide (Carborundum 440 mesh; Nacalai Tesque, Kyoto, Japan) in the presence of a minimum volume of buffer B (25 mM Tris-HCl, pH 7.6, 1 mM dithiothreitol, 1 mM sodium EDTA, 0.25 M sucrose, and EDTA-free Complete protease inhibitor mixture (Roche Applied Science)). The resultant cell paste was resuspended in buffer B and centrifuged at 500 × *g* for 5 min and 1000 × *g* for 15 min to remove silicon carbide and nuclear fraction, respectively. The mitochondrial fraction was recovered upon centrifugation of the last supernatant at 10,000 × *g* for 15 min, washed three times in buffer B, and resuspended to a protein concentration of ~30 mg/ml and kept at −80 °C until use.

TABLE 1
Purification of complex II from *T. cruzi* mitochondria

Step	Protein	Succinate:DCIP reductase	Yield	Purification
	mg	*units*	*units/mg*	*%*	*-fold*
Mitochondria	314	27	0.085	100	1.0
SML extract	141	22	0.16	83	1.9
Source 15Q	7.8	7.6	0.97	28	12
Superdex 200 (1st)	1.3	1.4	1.09	5.3	13
Superdex 200 (2nd)	0.15	0.43	2.87	1.6	34

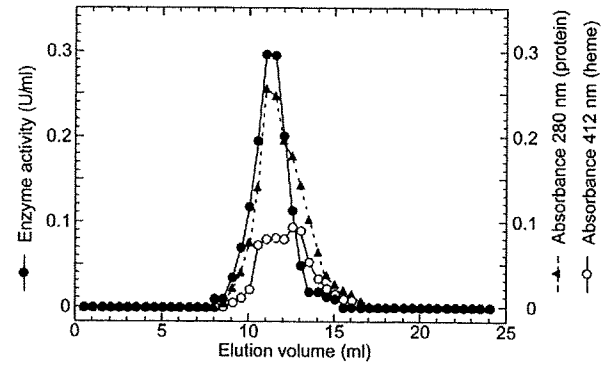

FIGURE 2. **Elution profile of *T. cruzi* Complex II on Superdex 200 chromatography.** Complex II fractions from the first gel filtration chromatography with a Superdex 200-pg column were concentrated and rechromatographed at the flow rate of 0.25 ml/min. Aliquots were collected every 0.5 ml. Elution profiles for proteins and cytochromes were monitored at 280 (▲) and 412 nm (○), respectively, and the enzyme activity (●) was measured as decylquinone-mediated succinate:DCIP reductase.

Isolation of Complex II—All steps were carried out at 4 °C. Mitochondrial fraction (~300 mg of protein from 10 liters culture) was brought to 70 ml with buffer C (10 mM KP_i, pH 7.5), 1 mM sodium EDTA, 1 mM sodium malonate, EDTA-free Complete protease inhibitor mixture (Roche Applied Science) (2 tablets/50 ml), 1% (w/v) sucrose monolaurate SM-1200 (SML) (Mitsubishi-Kagaku Foods Co., Tokyo, Japan)). The mixture was stirred for 30 min and centrifuged at 200,000 × *g* for 1 h. The supernatant was loaded at 1 ml/min onto a Source 15 Q column (1.6 inner diameter × 10 cm; GE Healthcare), equilibrated with buffer C containing 0.1% SML. After washing with 5 volumes of the same buffer, proteins were eluted with a 200-ml linear gradient of NaCl from 0 to 150 mM at 2 ml/min. Active fractions were concentrated to ~250 μl by ultrafiltration with Amicon Ultra-4 (molecular weight cutoff 100,000, Millipore) and subjected to gel filtration FPLC with a Superdex 200-pg 10/300 GL column (1 cm inner diameter × 30 cm; GE Healthcare) at 0.25 ml/min in 20 mM MOPS-NaOH, pH 7.2, containing 1 mM sodium EDTA, 1 mM sodium malonate, 150 mM NaCl, and 0.1% SML. Peak fractions were rechromatographed as above, and purified enzyme was concentrated and stored at −80 °C until use.

Identification of Complex II Subunits—The purified enzyme was subjected to 12.5% SDS-PAGE, and subunits were transferred to an Immobilon-P membrane (Millipore), followed by

staining with Coomassie Brilliant Blue R-250 (19, 20). Five or ten N-terminal amino acid residues were determined with a Procise 494 HT (Applied Biosystems) or an Hp G1005A (Hewlett-Packard Co.) Protein Sequencing System at the Bio-Medical Research Center of Juntendo University or APRO Life Science Institute, Inc. (Tokushima, Japan). When the N terminus was blocked, protein bands were digested with trypsin, and internal peptide sequences were determined (20). Genes coded for Complex II subunits were identified with BLASTP in the *T. cruzi* genome data base (15).

Phase Partitioning of Mitochondrial Fraction with Triton X-114—Phase partitioning by Triton X-114 was performed as described previously (21) with a slight modification. A total of 2–3 mg of mitochondrial fraction was resuspended in 1 ml of Tris-HCl, pH 7.5, 150 mM NaCl, 1 mM EDTA, 2 mM sodium malonate, Complete protease inhibitors mixture (Roche Applied Science) (2 tablets/50 ml), protease inhibitors mixture for mammalian cell and tissue extracts (Sigma) (10 μl/ml), and 2% (v/v) Triton X-114. The mixture was incubated for 30 min on ice and kept at −30 °C overnight. After thawing, the insoluble material was removed by centrifugation at 4 °C, and the supernatant was incubated for 10 min at 37 °C and centrifuged at 2000 × *g* for 10 min to separate the aqueous and detergent-rich phases. The aqueous phase was brought to 2% (v/v) Triton X-114, whereas the detergent-rich fraction was brought to 1 ml with the above buffer. After incubation on ice for 10 min, samples were incubated at 37 °C for 10 min and phases separated as before. This wash step was repeated three times. Finally, the samples were dialyzed and concentrated by Amicon Ultra-4 (Millipore) in the presence of 50 mM imidazole, 50 mM NaCl, 6 mM aminocaproic acid, 0.05% (w/v) deoxycholate, and 0.1% (w/v) SML, pH 7, and kept at −80 °C until use.

Enzyme Assay—Decylubiquinone-mediated succinate-2,4 dichlorophenolindophenol (DCIP) reductase activity was measured at 25 °C in 100 mM potassium phosphate, pH 7.4, containing 1 mM $MgCl_2$, 2 mM KCN, 0.1 mM antimycin A (Sigma), and 0.1% SML with 63 μM decylubiquinone (Sigma) *plus* 60 μM DCIP. After 2 min of incubation, reduction of DCIP (ϵ_{600} = 21 mM^{-1} cm^{-1}) was measured in the presence of 10 mM succinate. SQR activity was determined with 40 μM ubiquinone-2 (Q_2) (Sigma, ϵ_{278} = 12.3 mM^{-1} cm^{-1}). Kinetic analysis was done with KaleidaGraph version 4.0 (Synergy Software).

Miscellaneous—High resolution clear native electrophoresis (hrCNE) (22) was performed with 4–16% Novex gels (Invitrogen) using 0.02% dodecylmaltoside and 0.05% sodium deoxycholate for the cathode buffer additives, and the Complex II band was visualized by the activity staining (23) or Coomassie Brilliant Blue. Tricine-PAGE analysis was done with Novex 10–20% Tricine gels (Invitrogen), and proteins bands were sequentially stained by Sypro ruby (Invitrogen) and silver. During purification the succinate-decylubiquinone-DCIP reduc-

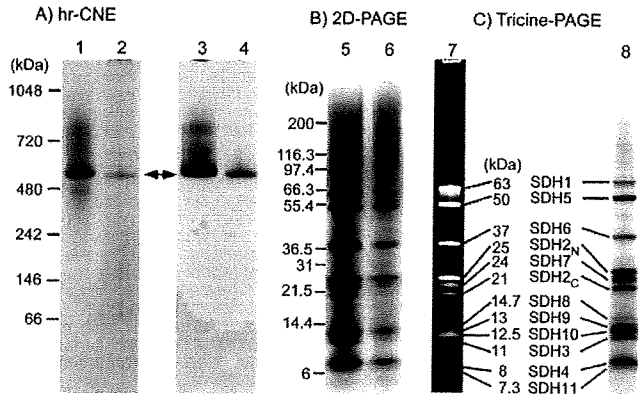

FIGURE 3. **Electrophoresis analysis of *T. cruzi* Complex II.** *A*, purified Complex II (2 μg; *lanes 1* and *3*) and the detergent-rich fraction from the phase partitioning by Triton X-114 of the mitochondrial fraction (60 μg; *lines 2* and *4*) were subjected to hrCNE. Proteins were stained by Coomassie Brilliant Blue (*left panel*), and Complex II was visualized by SDH activity staining (*right panel*). *B*, proteins of Complex II showing SDH activity in *A* were analyzed by 10–20% Tricine SDS-PAGE and visualized by silver stain (*lane 5*, pure complex; *lane 6*, detergent-rich fraction). *C* shows the subunit composition of the pure Complex II from *T. cruzi* stained by SYPRO ruby (*lane 7*) or silver stain (*lane 8*). Molecular weight standards used are NativeMark (Invitrogen, *lane 1*) and Mark 12 unstained standards (Invitrogen, *lanes 5* and *7*).

TABLE 2
Identification of genes encoding subunits for *T. cruzi* complex II

Subunit[a]	Sequence confirmed[b]	Accession number or RefSeq ID at NCBI (haplotype,[c] M_r)	Identity[d]	TM[e]
			%	
SDH1	Ser^{10}–Met^{19}	AB031741 (NE, 66,974), XP_809281 (E, 18,231)	59	0
SDH5	Ala^{10}–Leu^{19}	XP_818124 (NE, 53,831), XP_810172 (E, 20,788)	16	0
$SDH2_N$	Ser^{188}–Arg^{196}, Lys^{201}–Ile^{204}, Gly^{221}–Asn^{223}, Glu^{267}–Ile^{269}	XP_814994 (merged, 32,232)[f]	24 (37)	0
$SDH2_C$	Pro^{2}–Leu^{6}	XP_803796 (NE, 21,352), XP_806126 (E, 21,379)	25 (43)	0
SDH6a	Val^{19}–Val^{28}	XP_809065 (NA, 36,077), XP_812789 (NA, 36,035)	15	0
SDH6b	Val^{19}–Val^{28}	XP_813603 (NA, 36,133), XP_813645 (NA, 36,039)	14	0
SDH7	Ile^{26}–Leu^{35}	XP_813318 (NE, 28,218), XP_820239 (E, 28,202)	22	0
SDH3	Val^{2}–Phe^{11}	XP_809410 (NE, 12,176), XP_810064 (E, 12,204)	29	1
SDH4	Phe^{39}–Thr^{48}	XP_808211 (E, 13,957), XP_816430 (NE, 13,975)	27	2
SDH8	Gly^{5}–Met^{16}	XP_809192 (NE, 16,199), XP_817545 (E, 16,143)	ND[g]	2
SDH9	Ile^{10}–Pro^{19}	XP_807105 (merged, 15,736)	ND	1
SDH10	Pro^{25}–Val^{33}	XP_808894 (NE, 15,565), XP_808903 (E, 15,554)	ND	1
SDH11	Phe^{20}–Cys^{29}	XP_814088 (E, 10,346), XP_814509 (NE, 10,337)	ND	1

[a] Alleles were named as SDH3-1 (XP_809410) and SDH3-2 (XP_810064) in the order of the accession numbers, except for SDH5.
[b] These are N-terminal sequences except for $SDH2_N$ and SDH8, where the N-terminal residues were blocked.
[c] Homozygous alleles located in a merged assembly of Esmeraldo (E) and non-Esmeraldo (NE) homologous sequences whose different copies were merged genes during the genome assembly are indicated by "merged." Haplotypes for gene with more than two copies in the genome that does not belong to a merged region are not assigned (NA).
[d] Identity % to counterparts in human were as follows: SDH1 (D30648), SDH2 (P21912), SDH3 (Q99643), or SDH4 (O14521). In parentheses, the identity % of $SDH2_N$ and $SDH2_C$ that correspond to either Met^{1}–Pro^{155} (Ip_N domain) or Tyr^{156}–Val^{280} (Ip_C domain), respectively, of human SDH2 is shown. Identity % for truncated forms of SDH1 and SDH5 (SDH1-2 and SDH5-2) in the Esmeraldo haplotype was 66 and 20%, respectively.
[e] Transmembrane segments (TM) were estimated with TMHMM (52) and SOSUI (53).
[f] SDH2N from other trypanosomatids lack Met^{1} to Arg^{42} of $TcSDH2_N$.
[g] ND indicates not determined because these hydrophobic sequences are a highly divergent form of mammalian sequences.

12-Subunit Complex II from T. cruzi

FIGURE 4. **Alignment of heterodimeric SDH2 sequences.** Amino acid residues proposed for binding of the iron-sulfur clusters are shown in *red* and those for the quinone binding in *blue*. Residue numbers refer to the *E. coli* SDH2 (SdhB) sequence. GenBank™ accession numbers for $SDH2_N$ and $SDH2_C$ sequences used are *T. cruzi* (XP_814994 and XP_803796), *T. brucei* (XP_847169 and XP_826981), and *L. major* (XP_001683488 and XP_001682013). Other SDH2 sequences used are *E. coli* (NP_415252), *Rickettsia prowazekii* (Q9ZEA1), *Reclinomonas americana* (NP_044798), *Dictyostelium discoideum* (XP_646559), *Plasmodium falciparum* (D86574), *Tetrahymena thermophila* (XP_001024894), *S. cerevisiae* (NP_012774), *Caenorhabditis elegans* (NP_495992), *H. sapiens* (NP_002991), and *A. thaliana* (NP_189374).

tase activity was monitored in a microplate spectrophotometer (Benchmark Plus, Bio-Rad). Kinetics and UV-visible absorption spectra were determined at room temperature with a V-660 UV-visible spectrophotometer (Jasco, Tokyo, Japan). Protoheme IX and protein concentrations were determined by pyridine hemochromogen method (24) and the micro BCA method (Pierce), respectively. Sequence alignment was done with ClustalX 2.0 (25).

RESULTS AND DISCUSSION

Isolation of T. cruzi Complex II—To determine the molecular organization of *T. cruzi* Complex II, we purified this enzyme from epimastigote mitochondria by ion-exchange and gel filtration chromatography using the nonionic detergent sucrose monolaurate (Table 1). Decylubiquinone-mediated succinate: DCIP reductase activity was eluted as a single peak at each step

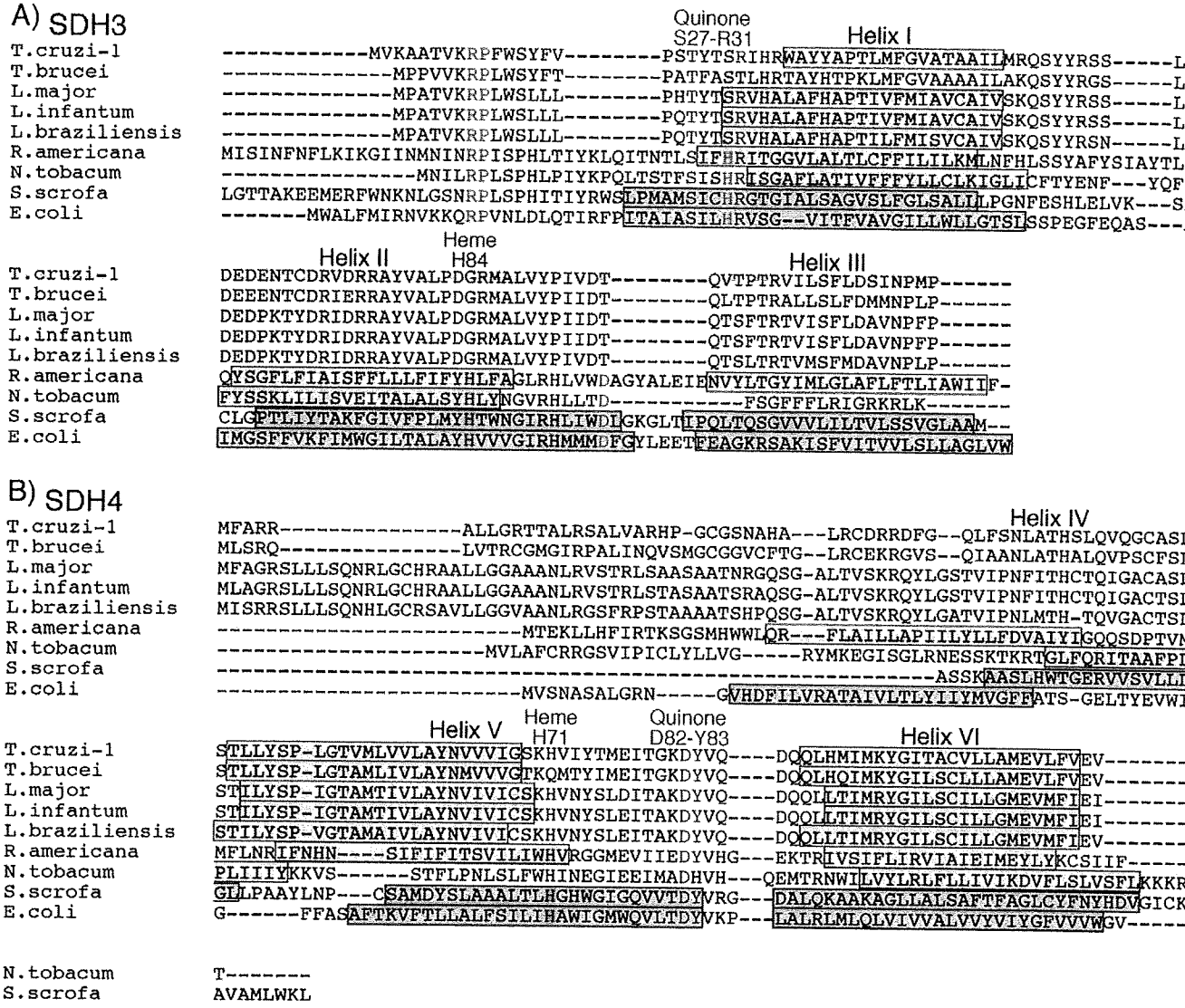

FIGURE 5. **Alignments of SDH3 (*A*) and SDH4 (*B*) sequences.** Amino acid residues proposed for binding of protoheme IX are shown in *red* and those for the quinone binding in *blue*. Other conserved residues are indicated by *green*. Transmembrane helices found in *E. coli* (Protein Data Bank code 1NEK) and porcine (Protein Data Bank code 1ZOY) Complex II are shown by *red rectangles*, and transmembrane helices predicted by TMHMM are indicated by *blue rectangles*. TMHMM failed to predict transmembrane helices in *T. brucei* SDH3. Residue numbers refer to *E. coli* SDH3 (SdhC) and SDH4 (SdhD). GenBank™ accession numbers for SDH3 and SDH4 sequences used are *T. cruzi* (XP_809410, XP_808211), *T. brucei* (XP_845531, XP_823384), *L. major* (XP_001684890, XP_001685874), *L. infantum* (XP_001467132), *L. brasiliensis* (XP_001566908, XP_001567905), *R. americana* (NP_044796, NP_044797), *Nicotiana tobacum* (YP_173376, YP_173457), *Sus scrofa* (1ZOY_C, 1ZOY_D), and *E. coli* (NP_415249, NP_415250).

and co-eluted with proteins and *b*-type cytochrome(s) at the second Superdex 200 chromatography (Fig. 2). Specific activity was increased 34-fold to 2.9 units/mg proteins, and the yield was ~2%. A hrCNE of the pure protein identified *T. cruzi* Complex II as an ~550-kDa complex (Fig. 3, *lanes 1* and *3*), which is 4-fold larger than bovine and yeast Complex II (130 kDa) and potato Complex II (150 kDa) (26, 27). Upon phase partitioning of the mitochondrial fraction with Triton X-114, the Complex II of *T. cruzi* was found only in the detergent-rich fraction (data not shown). Analysis of the detergent-rich fraction by hrCNE showed the Complex II as a single band at the same position as the pure enzyme (~550 kDa) (Fig. 3, *lanes 2* and *4*). These results indicated that the purified Complex II was obtained in its intact form. Interestingly, second dimensional analysis of both the purified Complex II and the detergent-rich fraction from phase partitioning with Triton X-114 with SDH activity showed that *T. cruzi* Complex II is composed of 12 subunits (Fig. 3, *lanes 5* and *6*). The same subunit composition was obtained by immunoaffinity purification of the partially purified enzyme (data not shown). The apparent molecular weight of the subunits ranges from 7.3 to 63 kDa (Fig. 3, *lanes 7* and *8*). Assuming the presence of equimolar amounts of subunits, a total molecular mass of Complex II would be 286.5 kDa, indicating that *T. cruzi* Complex II is a homodimer.

Identification of Genes Coded for Subunits—We determined N-terminal sequences (or internal peptide sequences in case of $SDH2_N$ and SDH8) of all subunits and identified genes coded for SDH1-1, $SDH2_N$, $SDH2_C$, SDH5–SDH7 (hydrophilic sub-

units), SDH3, SDH4, and SDH8–SDH11 (hydrophobic subunits) (Table 2). All subunits, except SDH1-1, are trypanosomatid-specific and structurally unrelated to plant-specific soluble subunits (AtSDH5–AtSDH8, 5–18 kDa) (27–29). All genes (except SDH6 with four copies) are present as two copies, which are assigned to either Esmeraldo or non-Esmeraldo haplotype (haploid genotype) in *T. cruzi* subgroup IIe. In contrast, only one copy each of the orthologues is present in *T. brucei*, *Leishmania major*, *Leishmania infantum*, and *Leishmania braziliensis* (supplemental Table S1). N-terminal sequence analysis of SDH3 and SDH7 showed that yields of two isoforms are similar (*i.e.* SDH3-1:SDH3-2 = 63:37, and SDH7-1:SDH7-2 = 54:46), indicating that isoforms are expressed from each haplotype. Because truncated isoforms for SDH1 and SDH5 in the Esmeraldo haplotype (see below) are not assembled into the 12-subunit complex and $SDH2_N$ and SDH9 isoforms have the identical sequence, 512 ($= 1^4 \times 4^1 \times 2^{(12-5)}$) kinds of heterogeneity may exist in the *T. cruzi* Complex II monomer (Table 2).

Flavoprotein Subunit—SDH1-1 (63-kDa band in Tricine-PAGE) cross-reacted with the antiserum against bovine SDH1 (data not shown) and is highly homologous to counterparts in *T. brucei* (93% identity), *L. major* (90%), *Homo sapiens* (59%), *Arabidopsis thaliana* (62%), *Saccharomyces cerevisiae* (61%), and *Escherichia coli* (48%, SdhA). Amino acid residues proposed for dicarboxylate binding and a FAD ligand histidine (12–14) are all conserved in SDH1-1. SDH1-1 and SDH5-1 of the non-Esmeraldo haplotype share a weak sequence similarity in the entire region, but the latter lacks amino acid residues responsible for FAD and dicarboxylate binding. In the Esmeraldo haplotype, SDH1-2 and SDH5-2 are truncated and contain only Met^1 to Gly^{167} of TcSDH1-1 and Ile^{305} to Met^{486} of TcSDH5-1, respectively (Table 2). These findings suggest that TcSDH1-1, TcSDH1-2, TcSDH5-1, and TcSDH5-2 might have evolved by gene duplication and subsequent degeneration.

Iron-Sulfur Subunit—Sequence analysis of the 25- and 21-kDa band proteins revealed that they contain the plant ferredoxin domain (Ip_N) and bacterial ferredoxin domain (Ip_C) of canonical SDH2 (Ip) in the N- and C-terminal half, respectively (Fig. 4). Sequence identities of Ip_N and Ip_C are 37 and 43%, respectively, to those of human SDH2 (Table 2), and the Ip_N and Ip_C domains contain all amino acid residues responsible for binding of iron-sulfur clusters and ubiquinone (12, 13, 30) (Fig. 4). Such a heterodimeric Ip subunit can be found in *T. brucei* (31), *T. cruzi*, *L. major*, *L. infantum*, and *L. brasiliensis* (Tables 2), which belong to the order Trypanosomatida. Thus we named these subunits as $SDH2_N$ and $SDH2_C$, respectively.

Splitting of mitochondrial membrane proteins has been reported for cytochrome *c* oxidase CoxII in Apicomplexa and Chlorophyceae (32, 33), and ATP synthase α subunit in *Leishmania tarentolae* and *T. brucei* (34, 35). The former occurs at the gene level and the latter by post-translational cleavage. Sequence analysis indicates that heterodimeric SDH2 and CoxII have emerged from gene duplication followed by degeneration of the N- or C-terminal half of the duplication products. Conserved domains in degenerated duplicons, which have arisen from mitochondrion-to-nucleus transfer of the duplicated genes (32, 33, 36), must retain the potential for protein-protein interactions and constitute a heterodimeric functional subunit by trans-complementation.

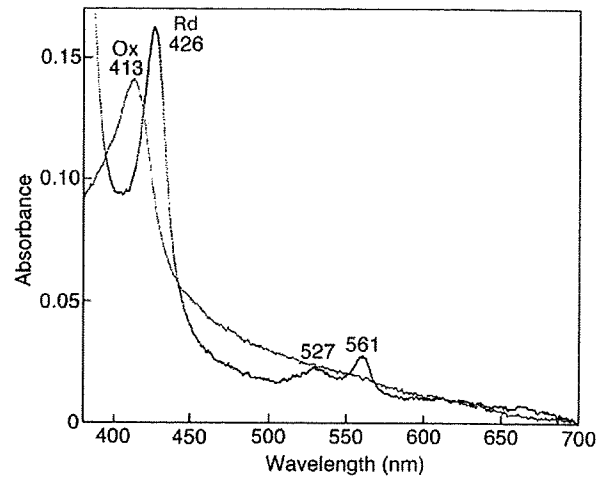

FIGURE 6. **Visible absorption spectra of *T. cruzi* Complex II.** Purified Complex II was desalted by ultrafiltration and diluted with 0.1 M sodium phosphate, pH 7.2, containing 0.1% SML at a final concentration of 0.06 mg/ml. Absorption spectra of the air-oxidized (*Ox, thin line*) and dithionite-reduced (*Rd, thick line*) forms were recorded at room temperature with UV-2400 spectrophotometer (Shimadzu Corp., Kyoto, Japan).

Membrane Anchor Subunits—Membrane anchor subunits in protist enzymes are highly divergent from bacterial and mammalian counterparts and difficult to find with conventional BLAST programs. We identified candidates for *T. cruzi* SDH3 and SDH4 by the presence of the quinone/heme-binding motifs "$RPX_{16}SX_2HR$ (SDH3 helix I)" and "$HX_{10}DY$ (SDH4 helix V)," respectively, present in membrane anchor subunits. In Complex II, Trp^{164} in SDH2 (Fig. 4) and Tyr^{83} in the SDH4 $HX_{10}DY$ motif (Fig. 5*B*) (*E. coli* numbering) could hydrogen bond to the O-1 atom of ubiquinone and contribute to the binding affinity (12, 37). Arg^{31} in the SDH3 SX_2HR motif (Fig. 5*A*) and Asp^{82} in the SDH4 $HX_{10}DY$ motif are in close proximity to ubiquinone and could interact with Tyr^{83} (37). Ser^{27} in the SDH3 SX_2HR motif has been shown to be essential for quinone binding (38) and is a candidate for hydrogen bonding to the O-4 atom of ubiquinone (30). The first arginine (Arg^9 in *E. coli* SDH3) in the $RPX_{16}SX_3R$ motif is in the vicinity of Glu^{186} in SDH1 and Asp^{106} in SDH2 and may play a structural role by making a hydrogen bond network.

In *T. cruzi*, SDH3 has the "$RPX_{11}SX_2HR$ motif in front of the predicted transmembrane helix I and lacks transmembrane helices II and III. However, sequence alignment suggests the presence of the alternative motif "$TX_2SR/(T)$" in the Trypanosomatida (Fig. 5*A*). In mitochondrial Complex II, protoheme IX is ligated by two His residues in the second transmembrane helix of SDH3 ("$HX_{10}D$" motif) and SDH4 ("$HX_{10}DY$" motif). A heme ligand in helix II (His^{84} in *E. coli* SDH3) may be substituted by a nearby histidine in the quinone-binding motif "SX_2HR" (39). In contrast, SDH4 lacks helix IV and appears to interact with heme and ubiquinone with the $HX_{10}DY$ motif. As in rice SDH4 (GenBank™ accession number NP_001045324), the heme ligand His is substituted by Gln in *T. brucei* SDH4. The presence of a bound heme or an alternative ligand in *T.*

brucei SDH4 needs to be tested in future studies. It is also possible that trypanosomatid-specific subunits could be assembled as a jigsaw puzzle-like membrane anchor.

Spectroscopic Properties of T. cruzi Complex II—Pyridine ferrohemochrome analysis showed that *T. cruzi* Complex II binds a stoichiometric amount of protoheme IX (0.85 heme/monomer of enzyme) indicating that monomer enzyme complex contains one heme. At room temperature, the air-oxidized and fully reduced forms of the purified enzyme showed peaks at 413 and 426, 527, and 561 nm, respectively (Fig. 6). Peak positions are similar to those reported for Complex II from *E. coli* (40), adult *A. suum* (41), and bovine (42, 43), where heme is ligated via histidine in the second helices of SDH3 and SDH4. Although heme has an important role in the assembly of Complex II, it is not essential for the reduction of ubiquinones (43, 44).

Enzymatic Properties of T. cruzi Complex II—We examined SQR activity of the purified enzyme and found the difference in apparent K_m values between Q_1 (33.9 ± 3.6 μM) and Q_2 (18.8 ± 6.4 μM) (Fig. 7), indicating that the 6-polyprenyl group of ubiquinone contributes to the binding affinity. The apparent V_{max} value of the *T. cruzi* Complex II was rather constant, 11.9 ± 2.2 for Q_1 and 11.5 ± 0.4 Q_2 units/mg proteins, respectively, and one-fourth of those reported for bovine and *E. coli* enzymes (45, 46). This is not surprising because *T. cruzi* complex II has about 2–3 times more proteins than the other enzymes. K_m values for ubiquinone and succinate (18.8 ± 6.4 μM (Q_2) and 1.48 ± 0.17 mM, respectively) were higher than 0.3 and 130 μM, respectively, of bovine enzyme (45), and 2 and 277 μM, respectively, of the *E. coli* enzyme (46, 47). Notably, the K_m value for succinate was comparable with 610 μM in adult *A. suum* (10), which expresses the stage-specific Complex II as quinol:fumarate reductase under hypoxic habitats in host organisms.

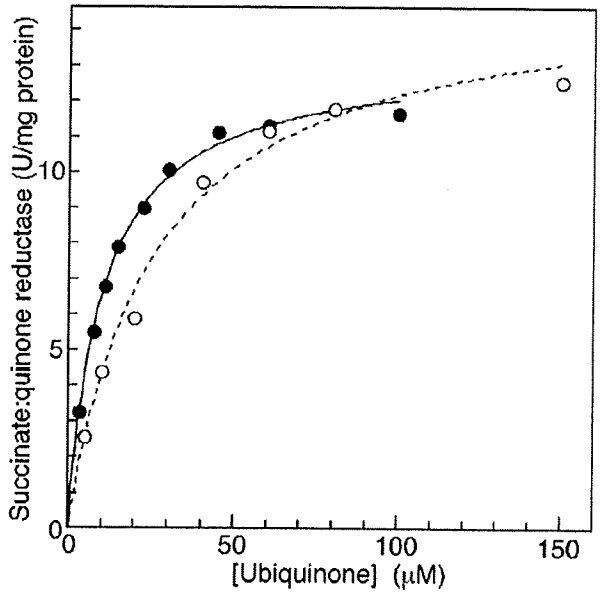

FIGURE 7. **Kinetic analysis of succinate-quinone reductase activity.** Succinate:ubiquinone reductase activity of the purified Complex II was determined with Q_1 (○) and Q_2 (●) at a protein concentration of 1.25 μg/ml in the presence of 10 mM sodium succinate. Data were fitted with the Michaelis-Menten equation using KaleidaGraph, and apparent K_m and V_{max} values were 30.3 ± 4.3 μM and 14.0 ± 1.2 units/mg protein, respectively, for Q_1 and 12.4 ± 0.7 μM and 11.9 ± 0.3 units/mg protein, respectively, for Q_2.

Then we examined effects of inhibitors for binding sites of quinones and dicarboxylates on SQR activity. Atpenin A5, a potent inhibitor for Complex II, inhibited the *T. cruzi* enzyme with the IC_{50} value of 6.4 ± 2.4 μM, which is 3 orders of magnitude higher than that of bovine Complex II (4 nM) (48). Furthermore, carboxin, 2-theonyltrifluoroacetone, plumbagin, and 2-heptyl-4-hydroxyquinoline *N*-oxide were ineffective (100 μM < IC_{50}). Structural divergence in trypanosomatid SDH3 and SDH4 could be the cause for lower binding affinities for both quinones and inhibitors. In addition, we found for the dicarboxylate-binding site that the IC_{50} value for malonate (40 μM) was much higher than the K_i value for bovine Complex II (1.3 μM) (45).

Structure of Trypanosomatid Complex II—To the best of our knowledge, this is the first report on the isolation of protist Complex II. *T. cruzi* Complex II has unusual subunit organization with six each of hydrophilic and hydrophobic subunits. Such a supramolecular structure and heterodimeric SDH2 ($SDH2_N$ and $SDH2_C$) are conserved in the Trypanosomatida. Furthermore, SDH1, $SDH2_N$, $SDH2_C$, SDH3, SDH4, and SDH8–SDH10 can be identified in the ongoing genome projects on the evolutionary relatives, the photosynthetic free-living *Euglena gracilis*, and the nonphotosynthetic euglenoid *Astasia longa* in the Euglenida. Thus a part of these features are common in the Euglenozoa, a divergent lineage of eukaryotes (Fig. 8).

Accumulation of noncatalytic subunits through expanding the protein interaction network could be a driving force for protein evolution. Structural and catalytic features are unique, and thus this enzyme could be a potential target for novel chemotherapeutic agents for trypanosomiasis and leishmaniasis.

Conclusion—The parasitic protist *T. brucei* is a gold mine where unprecedented biological phenomena like RNA editing and trans-splicing in mitochondria were originally discovered. It was found recently in *Diplonema papillatum*, a free-living evolutionary cousin,

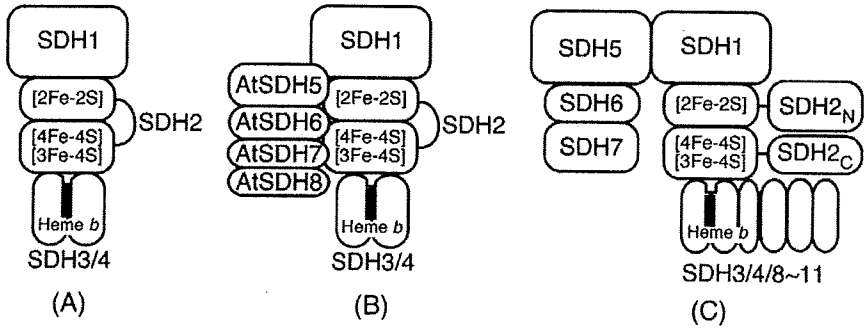

FIGURE 8. **Subunit organization of Complex II.** *A*, common four-subunit Complex II (*e.g.* mammals, *E. coli*); *B*, eight-subunit Complex II in plants (*e.g. A. thaliana*); and *C*, 12-subunit Complex II in the Trypanosomatida. Noncatalytic subunits and domains are shown in *yellow* and heme in *red*.

that mature mRNA for cytochrome *c* oxidase CoxI was assembled from nine gene fragments by a jigsaw puzzle mechanism (49). From a characterization of Complex II from *T. cruzi*, we revealed a novel supramolecular organization, which is conserved in the Trypanosomatida.

Parasites have exploited unique energy metabolic pathways as adaptations to their natural habitats within their hosts (50, 51). In fact, the respiratory systems of parasites typically show greater diversity in electron transfer pathways than those of host animals. As shown in this study, such is also the case with Complex II, which is a well known marker enzyme of mitochondria. Studies on the role of supramolecular Complex II in adaptation of trypanosomatids is now underway in our laboratory.

Acknowledgments—We thank Drs. J. L. Concepcion (Universidad de Los Andes, Merida-Venezuela) and T. Nara (Juntendo University) for kind advice; and Drs. M. Matsuzaki (University of Tokyo), T. Hashimoto (University of Tsukuba), G. Cecchini (University of California San Francisco), and M. Müller (Rockefeller University) for critical reading of the manuscript.

REFERENCES

1. World Health Organization (2007) *Report of the First Meeting of WHO Strategic and Technical Advisory Group on Neglected Tropical Diseases,* pp. 1–26, Geneva, Switzerland
2. Berriman, M., Ghedin, E., Hertz-Fowler, C., Blandin, G., Renauld, H., Bartholomeu, D. C., Lennard, N. J., Caler, E., Hamlin, N. E., Haas, B., Bohme, U., Hannick, L., Aslett, M. A., Shallom, J., Marcello, L., Hou, L., Wickstead, B., Alsmark, U. C., Arrowsmith, C., Atkin, R. J., Barron, A. J., Bringaud, F., Brooks, K., Carrington, M., Cherevach, I., Chillingworth, T. J., Churcher, C., Clark, L. N., Corton, C. H., Cronin, A., Davies, R. M., Doggett, J., Djikeng, A., Feldblyum, T., Field, M. C., Fraser, A., Goodhead, I., Hance, Z., Harper, D., Harris, B. R., Hauser, H., Hostetler, J., Ivens, A., Jagels, K., Johnson, D., Johnson, J., Jones, K., Kerhornou, A. X., Koo, H., Larke, N., Landfear, S., Larkin, C., Leech, V., Line, A., Lord, A., Macleod, A., Mooney, P. J., Moule, S., Martin, D. M., Morgan, G. W., Mungall, K., Norbertczak, H., Ormond, D., Pai, G., Peacock, C. S., Peterson, J., Quail, M. A., Rabbinowitsch, E., Rajandream, M. A., Reitter, C., Salzberg, S. L., Sanders, M., Schobel, S., Sharp, S., Simmonds, M., Simpson, A. J., Tallon, L., Turner, C. M., Tait, A., Tivey, A. R., Van Aken, S., Walker, D., Wanless, D., Wang, S., White, B., White, O., Whitehead, S., Woodward, J., Wortman, J., Adams, M. D., Embley, T. M., Gull, K., Ullu, E., Barry, J. D., Fairlamb, A. H., Opperdoes, F., Barrell, B. G., Donelson, J. E., Hall, N., Fraser, C. M., Melville, S. E., and El-Sayed, N. M. (2005) *Science* **309,** 416–422
3. Cazzulo, J. J. (1994) *J. Bioenerg. Biomembr.* **26,** 157–165
4. Besteiro, S., Barrett, M. P., Riviere, L., and Bringaud, F. (2005) *Trends Parasitol.* **21,** 185–191
5. Bringaud, F., Riviere, L., and Coustou, V. (2006) *Mol. Biochem. Parasitol.* **149,** 1–9
6. Takashima, E., Inaoka, D. K., Osanai, A., Nara, T., Odaka, M., Aoki, T., Inaka, K., Harada, S., and Kita, K. (2002) *Mol. Biochem. Parasitol.* **122,** 189–200
7. Van Hellemond, J. J., Opperdoes, F. R., and Tielens, A. G. (1998) *Proc. Natl. Acad. Sci. U. S. A.* **95,** 3036–3041
8. Harington, J. S. (1961) *Parasitology* **51,** 309–318
9. Roos, M. H., and Tielens, A. G. (1994) *Mol. Biochem. Parasitol.* **66,** 273–281
10. Saruta, F., Kuramochi, T., Nakamura, K., Takamiya, S., Yu, Y., Aoki, T., Sekimizu, K., Kojima, S., and Kita, K. (1995) *J. Biol. Chem.* **270,** 928–932
11. Cecchini, G. (2003) *Annu. Rev. Biochem.* **72,** 77–109
12. Yankovskaya, V., Horsefield, R., Tornroth, S., Luna-Chavez, C., Miyoshi, H., Leger, C., Byrne, B., Cecchini, G., and Iwata, S. (2003) *Science* **299,** 700–704
13. Sun, F., Huo, X., Zhai, Y., Wang, A., Xu, J., Su, D., Bartlam, M., and Rao, Z. (2005) *Cell* **121,** 1043–1057
14. Huang, L. S., Sun, G., Cobessi, D., Wang, A. C., Shen, J. T., Tung, E. Y., Anderson, V. E., and Berry, E. A. (2006) *J. Biol. Chem.* **281,** 5965–5972
15. El-Sayed, N. M., Myler, P. J., Bartholomeu, D. C., Nilsson, D., Aggarwal, G., Tran, A. N., Ghedin, E., Worthey, E. A., Delcher, A. L., Blandin, G., Westenberger, S. J., Caler, E., Cerqueira, G. C., Branche, C., Haas, B., Anupama, A., Arner, E., Aslund, L., Attipoe, P., Bontempi, E., Bringaud, F., Burton, P., Cadag, E., Campbell, D. A., Carrington, M., Crabtree, J., Darban, H., da Silveira, J. F., de Jong, P., Edwards, K., Englund, P. T., Fazelina, G., Feldblyum, T., Ferella, M., Frasch, A. C., Gull, K., Horn, D., Hou, L., Huang, Y., Kindlund, E., Klingbeil, M., Kluge, S., Koo, H., Lacerda, D., Levin, M. J., Lorenzi, H., Louie, T., Machado, C. R., McCulloch, R., McKenna, A., Mizuno, Y., Mottram, J. C., Nelson, S., Ochaya, S., Osoegawa, K., Pai, G., Parsons, M., Pentony, M., Pettersson, U., Pop, M., Ramirez, J. L., Rinta, J., Robertson, L., Salzberg, S. L., Sanchez, D. O., Seyler, A., Sharma, R., Shetty, J., Simpson, A. J., Sisk, E., Tammi, M. T., Tarleton, R., Teixeira, S., Van Aken, S., Vogt, C., Ward, P. N., Wickstead, B., Wortman, J., White, O., Fraser, C. M., Stuart, K. D., and Andersson, B. (2005) *Science* **309,** 409–415
16. Ivens, A. C., Peacock, C. S., Worthey, E. A., Murphy, L., Aggarwal, G., Berriman, M., Sisk, E., Rajandream, M. A., Adlem, E., Aert, R., Anupama, A., Apostolou, Z., Attipoe, P., Bason, N., Bauser, C., Beck, A., Beverley, S. M., Bianchettin, G., Borzym, K., Bothe, G., Bruschi, C. V., Collins, M., Cadag, E., Ciarloni, L., Clayton, C., Coulson, R. M., Cronin, A., Cruz, A. K., Davies, R. M., De Gaudenzi, J., Dobson, D. E., Duesterhoeft, A., Fazelina, G., Fosker, N., Frasch, A. C., Fraser, A., Fuchs, M., Gabel, C., Goble, A., Goffeau, A., Harris, D., Hertz-Fowler, C., Hilbert, H., Horn, D., Huang, Y., Klages, S., Knights, A., Kube, M., Larke, N., Litvin, L., Lord, A., Louie, T., Marra, M., Masuy, D., Matthews, K., Michaeli, S., Mottram, J. C., Muller-Auer, S., Munden, H., Nelson, S., Norbertczak, H., Oliver, K., O'Neil, S., Pentony, M., Pohl, T. M., Price, C., Purnelle, B., Quail, M. A., Rabbinowitsch, E., Reinhardt, R., Rieger, M., Rinta, J., Robben, J., Robertson, L., Ruiz, J. C., Rutter, S., Saunders, D., Schafer, M., Schein, J., Schwartz, D. C., Seeger, K., Seyler, A., Sharp, S., Shin, H., Sivam, D., Squares, R., Squares, S., Tosato, V., Vogt, C., Volckaert, G., Wambutt, R., Warren, T., Wedler, H., Woodward, J., Zhou, S., Zimmermann, W., Smith, D. F., Blackwell, J. M., Stuart, K. D., Barrell, B., and Myler, P. J. (2005) *Science* **309,** 436–442
17. Bourguignon, S. C., Mello, C. B., Santos, D. O., Gonzalez, M. S., and Souto-Padron, T. (2006) *Acta Trop.* **98,** 103–109
18. Concepcion, J. L., Chataing, B., and Dubourdieu, M. (1999) *Comp. Biochem. Physiol.* **122,** 211–222
19. Matsudaira, P. (1987) *J. Biol. Chem.* **262,** 10035–10038
20. Rosenfeld, J., Capdevielle, J., Guillemot, J. C., and Ferrara, P. (1992) *Anal. Biochem.* **203,** 173–179
21. Brusca, J. S., and Radolf, J. D. (1994) *Methods Enzymol.* **228,** 182–193
22. Wittig, I., Karas, M., and Schagger, H. (2007) *Mol. Cell. Proteomics* **6,** 1215–1225
23. Sabar, M., Balk, J., and Leaver, C. J. (2005) *Plant J.* **44,** 893–901
24. Berry, E. A., and Trumpower, B. L. (1987) *Anal. Biochem.* **161,** 1–15
25. Larkin, M. A., Blackshields, G., Brown, N. P., Chenna, R., McGettigan, P. A., McWilliam, H., Valentin, F., Wallace, I. M., Wilm, A., Lopez, R., Thompson, J. D., Gibson, T. J., and Higgins, D. G. (2007) *Bioinformatics (Oxf.)* **23,** 2947–2948
26. Schagger, H., and Pfeiffer, K. (2000) *EMBO J.* **19,** 1777–1783
27. Millar, A. H., Eubel, H., Jansch, L., Kruft, V., Heazlewood, J. L., and Braun, H. P. (2004) *Plant Mol. Biol.* **56,** 77–90
28. Eubel, H., Heinemeyer, J., and Braun, H. P. (2004) *Plant Physiol.* **134,** 1450–1459
29. Eubel, H., Heinemeyer, J., Sunderhaus, S., and Braun, H. P. (2004) *Plant Physiol. Biochem.* **42,** 937–942
30. Horsefield, R., Yankovskaya, V., Sexton, G., Whittingham, W., Shiomi, K., Omura, S., Byrne, B., Cecchini, G., and Iwata, S. (2006) *J. Biol. Chem.* **281,** 7309–7316
31. Allen, J. W., Ginger, M. L., and Ferguson, S. J. (2004) *Biochem. J.* **383,** 537–542
32. Funes, S., Davidson, E., Reyes-Prieto, A., Magallon, S., Herion, P., King, M. P., and Gonzalez-Halphen, D. (2002) *Science* **298,** 2155

33. Waller, R. F., and Keeling, P. J. (2006) *Gene (Amst.)* **383,** 33–37
34. Williams, N., and Frank, P. H. (1990) *Mol. Biochem. Parasitol.* **43,** 125–132
35. Nelson, R. E., Aphasizheva, I., Falick, A. M., Nebohacova, M., and Simpson, L. (2004) *Mol. Biochem. Parasitol.* **135,** 221–224
36. Adams, K. L., Rosenblueth, M., Qiu, Y. L., and Palmer, J. D. (2001) *Genetics* **158,** 1289–1300
37. Tran, Q. M., Rothery, R. A., Maklashina, E., Cecchini, G., and Weiner, J. H. (2006) *J. Biol. Chem.* **281,** 32310–32317
38. Yang, X., Yu, L., He, D., and Yu, C. A. (1998) *J. Biol. Chem.* **273,** 31916–31923
39. Maklashina, E., Rothery, R. A., Weiner, J. H., and Cecchini, G. (2001) *J. Biol. Chem.* **276,** 18968–18976
40. Kita, K., Vibat, C. R., Meinhardt, S., Guest, J. R., and Gennis, R. B. (1989) *J. Biol. Chem.* **264,** 2672–2677
41. Takamiya, S., Furushima, R., and Oya, H. (1986) *Biochim. Biophys. Acta* **848,** 99–107
42. Tushurashvili, P. R., Gavrikova, E. V., Ledenev, A. N., and Vinogradov, A. D. (1985) *Biochim. Biophys. Acta* **809,** 145–159
43. Tran, Q. M., Rothery, R. A., Maklashina, E., Cecchini, G., and Weiner, J. H. (2007) *Proc. Natl. Acad. Sci. U. S. A.* **104,** 18007–18012
44. Oyedotun, K. S., Sit, C. S., and Lemire, B. D. (2007) *Biochim. Biophys. Acta* **1767,** 1436–1445
45. Grivennikova, V. G., Gavrikova, E. V., Timoshin, A. A., and Vinogradov, A. D. (1993) *Biochim. Biophys. Acta* **1140,** 282–292
46. Maklashina, E., and Cecchini, G. (1999) *Arch. Biochem. Biophys.* **369,** 223–232
47. Miyadera, H., Hiraishi, A., Miyoshi, H., Sakamoto, K., Mineki, R., Murayama, K., Nagashima, K. V., Matsuura, K., Kojima, S., and Kita, K. (2003) *Eur. J. Biochem.* **270,** 1863–1874
48. Miyadera, H., Shiomi, K., Ui, H., Yamaguchi, Y., Masuma, R., Tomoda, H., Miyoshi, H., Osanai, A., Kita, K., and Omura, S. (2003) *Proc. Natl. Acad. Sci. U. S. A.* **100,** 473–477
49. Marande, W., and Burger, G. (2007) *Science* **318,** 415
50. Kita, K., and Takamiya, S. (2002) *Adv. Parasitol.* **51,** 95–131
51. Tielens, A. G., Rotte, C., van Hellemond, J. J., and Martin, W. (2002) *Trends Biochem. Sci.* **27,** 564–572
52. Krogh, A., Larsson, B., von Heijne, G., and Sonnhammer, E. L. L. (2001) *J. Mol. Biol.* **305,** 567–580
53. Mitaku, S., Hirokawa, T., and Tsuji, T. (2002) *Bioinformatics* **18,** 608–616

electronic reprint

Acta Crystallographica Section F
Structural Biology and Crystallization Communications
ISSN 1744-3091
Editors: **H. M. Einspahr and M. S. Weiss**

Crystallization of mitochondrial rhodoquinol-fumarate reductase from the parasitic nematode *Ascaris suum* with the specific inhibitor flutolanil

Arihiro Osanai, Shigeharu Harada, Kimitoshi Sakamoto, Hironari Shimizu, Daniel Ken Inaoka and Kiyoshi Kita

Acta Cryst. (2009). F**65**, 941–944

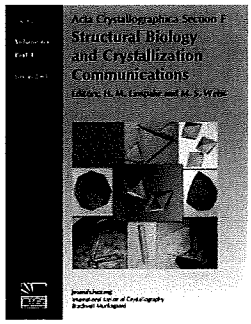

Acta Crystallographica Section F: Structural Biology and Crystallization Communications is a rapid all-electronic journal, which provides a home for short communications on the crystallization and structure of biological macromolecules. It includes four categories of publication: protein structure communications; nucleic acid structure communications; structural genomics communications; and crystallization communications. Structures determined through structural genomics initiatives or from iterative studies such as those used in the pharmaceutical industry are particularly welcomed. *Section F* is essential for all those interested in structural biology including molecular biologists, biochemists, crystallization specialists, structural biologists, biophysicists, pharmacologists and other life scientists.

Acta Crystallographica Section F
Structural Biology and Crystallization Communications
ISSN 1744-3091

Crystallization of mitochondrial rhodoquinol-fumarate reductase from the parasitic nematode *Ascaris suum* with the specific inhibitor flutolanil

Arihiro Osanai,[a] Shigeharu Harada,[b] Kimitoshi Sakamoto,[a]* Hironari Shimizu,[a] Daniel Ken Inaoka[a] and Kiyoshi Kita[a]

[a]Department of Biomedical Chemistry, Graduate School of Medicine, University of Tokyo, 7-3-1 Hongo, Bunkyo-ku, Tokyo 113-0033, Japan, and [b]Department of Applied Biology, Graduate School of Science and Technology, Kyoto Institute of Technology, Sakyo-ku, Kyoto 606-8585, Japan

Correspondence e-mail: sakamok@m.u-tokyo.ac.jp

Received 2 June 2009
Accepted 8 August 2009

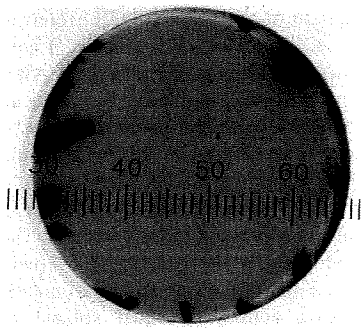

In adult *Ascaris suum* (roundworm) mitochondrial membrane-bound complex II acts as a rhodoquinol-fumarate reductase, which is the reverse reaction to that of mammalian complex II (succinate-ubiquinone reductase). The adult *A. suum* rhodoquinol-fumarate reductase was crystallized in the presence of octaethyleneglycol monododecyl ether and *n*-dodecyl-β-D-maltopyranoside in a 3:2 weight ratio. The crystals belonged to the orthorhombic space group $P2_12_12_1$, with unit-cell parameters $a = 123.75$, $b = 129.08$, $c = 221.12$ Å, and diffracted to 2.8 Å resolution using synchrotron radiation. The presence of two molecules in the asymmetric unit (120 kDa × 2) gives a crystal volume per protein mass (V_M) of 3.6 Å^3 Da^{-1}.

1. Introduction

In parasites, fumarate plays an important role in redox homeostasis. The parasitic protozoan *Trypanosoma cruzi* utilizes bacterial-type dihydroorotate dehydrogenase (TcDHOD), which is the fourth enzyme in the pyrimidine-biosynthesis pathway and catalyzes the oxidation of dihydroorotate and the reduction of fumarate to succinate. We have elucidated the catalytic mechanisms of these sequential reactions by determination of the three-dimensional structures of TcDHOD in the ligand-free form and in complex with the substrates (dihydroorotate and fumarate), product (orotate and succinate) and inhibitor (oxonate) at atomic resolution (Inaoka *et al.*, 2008).

In parasitic helminths, fumarate is the terminal electron acceptor of the anaerobic respiratory chain, which is essential for the survival of the parasites in the host (Kita & Takamiya, 2002). Complex II catalyzes fumarate reduction in anaerobic respiration and functions as a terminal oxidase. In eukaryotes, complex II (succinate-ubiquinone reductase in aerobic respiration; SQR) is located in the inner mitochondrial membrane and is generally composed of four polypeptides. The flavoprotein (Fp) subunit is the largest, with an approximate molecular mass of 70 kDa, and contains flavin adenine dinucleotide (FAD) as a prosthetic group. Complex II contains a relatively hydrophilic catalytic region formed by the Fp subunit and an iron–sulfur cluster (Ip) subunit, which has a molecular mass of approximately 30 kDa. The remaining subunits comprise cytochrome *b*, which contains a haem *b*. Cytochrome *b* is composed of two hydrophobic membrane-anchoring polypeptide subunits, namely a 15 kDa large subunit (CybL) and a 13 kDa small subunit (CybS). These cytochrome *b* subunits are necessary for the interaction of complex II with hydrophobic membrane-associated quinones such as ubiquinone (UQ) and rhodoquinone (RQ).

Our recent study on the respiratory chain of the parasitic nematode *Ascaris suum* has shown that the mitochondrial NADH-fumarate reductase system plays an important role in the anaerobic energy metabolism of adult parasites inhabiting hosts and that they undergo unique developmental changes during their life cycle (Kita & Takamiya, 2002; Iwata *et al.*, 2008). In anaerobic metabolism by *A. suum* mitochondria, the transfer of a reducing equivalent from NADH to the low-potential RQ is conducted by the NADH–RQ reductase complex (complex I). This pathway ends with the production of succinate by the rhodoquinol-fumarate reductase (QFR) activity of complex II. Electron transfer from NADH to fumarate is

coupled to site I phosphorylation of complex I *via* the generation of a proton gradient. The difference in redox potential between the NAD^+/NADH couple (E'_m = −320 mV) and the fumarate/succinate couple (E'_m = +30 mV) is sufficient to drive ATP synthesis.

The anaerobic NADH-fumarate reductase system is found not only in nematodes but also in bacteria and many other parasites and is a promising target for chemotherapy (Omura *et al.*, 2001; Tielens *et al.*, 2002; Matsumoto *et al.*, 2008). The most potent inhibitor of complex II, atpenin A5, was found during screening for inhibitors of *A. suum* complex II (Miyadera *et al.*, 2003). However, the mammalian complex II is much more sensitive to atpenin A5 than the *A. suum* enzyme. By further screening, we have found that flutolanil, a commercially available fungicide (Ito *et al.*, 2004), specifically inhibits the *A. suum* complex II. Therefore, we have taken flutolanil as a lead compound for structure-based drug design. In the current study, we have purified, crystallized and performed preliminary X-ray diffraction studies on the adult *A. suum* QFR.

2. Methods

2.1. Purification

Mitochondria were prepared from the muscle of adult *A. suum* as described by Takamiya *et al.* (1984), except that Chappell–Perry medium (100 m*M* KCl, 50 m*M* Tris–HCl pH 7.4, 1 m*M* ATP, 5 m*M* $MgSO_4$ and 1 m*M* EDTA; Ernster & Nordenbrand, 1967) was used instead of MSE medium (210 m*M* mannitol, 70 m*M* sucrose and 0.1 m*M* EDTA). The QFR was solubilized from adult *A. suum* mitochondria in 1.0%(*w*/*v*) sucrose monolaurate (Dojindo) and purified in the presence of 0.1%(*w*/*v*) sucrose monolaurate. *A. suum* mitochondria (1 g protein) were homogenized in 500 ml buffer *A* (10 m*M* Tris–HCl pH 7.5, 1 m*M* sodium malonate) containing 1.0%(*w*/*v*) sucrose monolaurate. After incubating the mixture for 30 min at 277 K, it was centrifuged for 1 h at 200 000*g*. The clear reddish-brown supernatant containing the solubilized QFR was applied onto a GE Healthcare DEAE Sepharose FF column (2.6 × 24 cm) pre-equilibrated with buffer *A* containing 0.1%(*w*/*v*) sucrose monolaurate. After washing the column with the same buffer, the QFR was eluted with 2400 ml of the buffer containing a linear gradient of 0.0–0.3 *M* NaCl. Fractions containing the QFR, which started to elute at approximately 0.1 *M* NaCl, were pooled and adjusted to 0.15 g ml^{-1} polyethylene glycol 3350 (Hampton Research) to precipitate the QFR. The mixture was centrifuged for 20 min at 15 000*g* and the precipitate was dissolved in buffer *A* containing 0.1%(*w*/*v*) sucrose monolaurate. The QFR was then further loaded onto a GE Healthcare Source 15Q column (1.6 × 10 cm) and eluted with 400 ml of buffer containing a linear gradient of 0–0.3 *M* NaCl. Fractions containing pure QFR as judged by SDS–PAGE (Fig. 1) were pooled. The purified QFR was then precipitated by adding solid polyethylene glycol (PEG) 3350 to 0.15 g ml^{-1} and stored at 193 K.

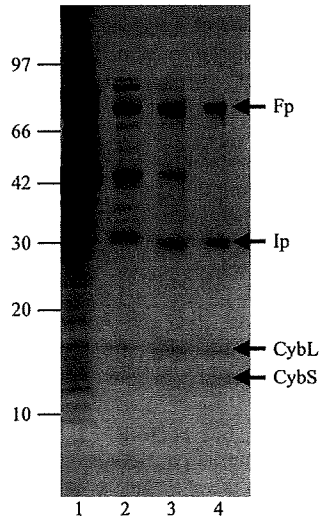

Figure 1
Purity of *A. suum* QFR at different stages of purification. Samples were separated by SDS–PAGE and the gel was stained with Coomassie Blue. The positions of molecular-weight markers are indicated on the left (in kDa) and the four subunits of *A. suum* QFR (Fp, flavoprotein subunit; Ip, iron–sulfur cluster subunit; CybL, cytochrome *b* large subunit; CybS, cytochrome *b* small subunit) are labelled on the right. Lane 1, whole mitochondria; lane 2, supernatant obtained after ultracentrifugation of the detergent extract; lane 3, pooled fractions from the DEAE Sepharose FF column; lane 4, pooled fractions from the Source 15Q column.

2.2. Crystallization

Conditions for crystallizing the *A. suum* QFR were screened using Crystal Screen (Jancarik & Kim, 1991) and Crystal Screen II (Hampton Research). Crystallization by hanging-drop vapour diffusion was carried out using 96-well CrystalClear Strips (Hampton Research). A droplet containing equal volumes of approximately 20 mg ml^{-1} QFR in buffer *A* containing detergent and reservoir solution was equilibrated against 100 µl reservoir solution.

Aggregates of microcrystals were observed at 293 K from reservoir solutions containing polyethylene glycols with medium molecular weights and 200 m*M* salts when octaethyleneglycol monododecyl ether (C12E8) was used as a detergent. Attempts to optimize the conditions by altering the PEG type (3350, 4000 and 6000), PEG concentration and pH and by using Additive Screen kits (Hampton Research) did not succeed in improving the crystallization. We therefore examined the effect of adding another detergent as an additive. 0.1 volume of detergent solution was added to a droplet of approximately 20 mg ml^{-1} QFR in buffer *A* containing 0.5%(*w*/*v*) C12E8 and an equal volume of reservoir solution and crystallization by hanging-drop vapour diffusion was carried out. After several days, small crystals (~10 µm; Fig. 2*a*) appeared at 293 K in drops from reservoir solutions composed of 14–18%(*w*/*v*) PEG 3350, 100 m*M* Tris–HCl pH 7.5–8.6, 200 m*M* NaCl and 1 m*M* sodium malonate when the drops included 0.3–0.5%(*w*/*v*) *n*-dodecyl-*β*-D-maltopyranoside (C12M). To determine the optimal ratio of C12E8 to C12M, crystallization was carried out using QFR dissolved in buffer *A* containing different concentrations of C12E8 and C12M. The best condition for crystallization (Fig. 2*b*) was achieved at a 3:2 C12E8:C12M weight ratio.

Crystals larger than 100 µm in size were grown by the microdialysis method as follows. The precipitate of the purified QFR stored at 193 K was dissolved in buffer *A* (approximately 10 mg ml^{-1}) containing 0.6%(*w*/*v*) C12E8, 0.4%(*w*/*v*) C12M and 200 m*M* NaCl. After incubation for 20 min on ice, the QFR was precipitated by adding an equal volume of 40%(*w*/*v*) PEG 3350. The precipitate obtained by centrifugation was dissolved in the same buffer, incubated for 20 min on ice and mixed with an equal volume of 40%(*w*/*v*) PEG 3350 to precipitate the QFR. This procedure was repeated several times in order to replace sucrose monolaurate with the added detergent. The precipitate was finally dissolved in buffer *A* containing 0.06%(*w*/*v*) C12E8, 0.04%(*w*/*v*) C12M and 0.2 *M* NaCl, giving an approximately 40 mg ml^{-1} QFR solution. After adding an equal volume of 23%(*w*/*v*) PEG 3350 to the QFR solution, undissolved materials were removed by centrifugation for 20 min at 20 000*g*. The supernatant was then sealed in a 5 µl microdialysis button and dialyzed against

reservoir solution containing 15.0%(*w*/*v*) PEG 3350, 100 m*M* Tris–HCl pH 8.4, 200 m*M* NaCl, 1 m*M* sodium malonate, 0.06%(*w*/*v*) C12E8 and 0.04%(*w*/*v*) C12M. Dark red plate-shaped crystals appeared within 24 h and grew to 100–200 µm after 2–3 d at 293 K (Fig. 2*c*).

X-ray diffraction data were collected on BL44XU at SPring-8 (Harima, Japan) and on BL-5A and NW12A at the Photon Factory (Tsukuba, Japan) by the rotation method. For X-ray diffraction experiments at 100 K, a QFR crystal mounted on a nylon loop was transferred successively to reservoir solution supplemented with 3.75, 7.5, 11.25 and 15% glycerol and was then frozen by rapid submergence in liquid nitrogen. Data were processed and scaled using *HKL*-2000 and *SCALEPACK* (Otwinowski & Minor, 1997).

3. Results and discussion

To obtain sufficient *A. suum* mitochondria for purification of the QFR, we slightly modified the standard protocol. Specifically, we used Chappell–Perry medium (Ernster & Nordenbrand, 1967) in place of the standard medium. This resulted in 0.95 mg mitochondria per gram of muscle and 0.3 µmol min^{-1} mg^{-1} mitochondrial succinate dehydrogenase activity, which represents a threefold increase in recovery and a fourfold increase in specific activity compared with the previous method (Takamiya *et al.*, 1984). Using this method, we obtained 7.5 mg pure enzyme (Fig. 1, lane 4) from 1 kg of adult *A. suum* muscle.

Because the success of membrane-protein crystallization strongly depends on which detergent is used, we tested a variety of commercially available nonionic detergents in the screening of crystallization conditions for the *A. suum* QFR. Aggregates of microcrystals were obtained under several crystallization conditions using the detergent C12E8, but we were unable to optimize the conditions. Instead, the optimal condition for producing crystals suitable for X-ray structure analysis was achieved when the sucrose monolaurate was exchanged for a 3:2 weight ratio of C12E8:C12M (Fig. 2*c*). Crystals grew to larger than 100 µm in 2–3 d by dialyzing QFR, which was dissolved in buffer *A* containing 11.5%(*w*/*v*) PEG 3350, 0.06%(*w*/*v*) C12E8, 0.04%(*w*/*v*) C12M and 200 m*M* NaCl, against reservoir solution containing 15.0%(*w*/*v*) PEG 3350, 100 m*M* Tris–HCl pH 8.4, 200 m*M* NaCl, 1 m*M* sodium malonate, 0.06%(*w*/*v*) C12E8 and 0.04%(*w*/*v*) C12M. Adding 11.5%(*w*/*v*) PEG 3350 to the QFR solution in advance prevented serious bubble formation in the microdialysis button, which was unfavourable for crystallization.

X-ray diffraction patterns were recorded from a single crystal at 100 K with an oscillation angle of 1.0° using a Bruker DIP-6040 imaging-plate detector on the BL44XU beamline at SPring-8. Analysis of the symmetry and the systematic absences in the recorded diffraction pattern indicated that the crystals belonged to the orthorhombic space group $P2_12_12_1$, with unit-cell parameters a = 123.75, b = 129.08, c = 221.12 Å. Assuming the presence of two QFR molecules (120 kDa × 2) in the asymmetric unit, the calculated Matthews coefficient V_M (Matthews, 1968) was 3.6 $Å^3$ Da^{-1}. A total of 587 189 observed reflections recorded on 180 images were merged to 75 372 unique reflections from 50.0 to 2.8 Å resolution.

During the screening of inhibitors, we found that flutolanil (Ito *et al.*, 2004), a commercially available fungicide, specifically inhibits *A. suum* SQR. The IC_{50} of flutolanil against *A. suum* and bovine SQR was 0.081 and 16 µ*M*, respectively, indicating that flutolanil is a promising lead compound for anthelminthics. To enable rational drug optimization, we prepared crystals of the *A. suum* QFR complexed with flutolanil by the soaking method. X-ray diffraction patterns were recorded at 100 K on 130 frames with an oscillation angle of 1° using an ADSC Quantum 315 CCD detector on NW12 at Photon Factory. A total of 54 964 unique reflections from 50.0 to 3.2 Å resolution were obtained. The data-collection and processing statistics are summarized in Table 1.

We attempted to solve the structure of the *A. suum* QFR by the molecular-replacement method using the *MOLREP* program (Navaza, 1994) as implemented within *CCP*4 (Collaborative Computational Project, Number 4, 1994) and the refined coordinates

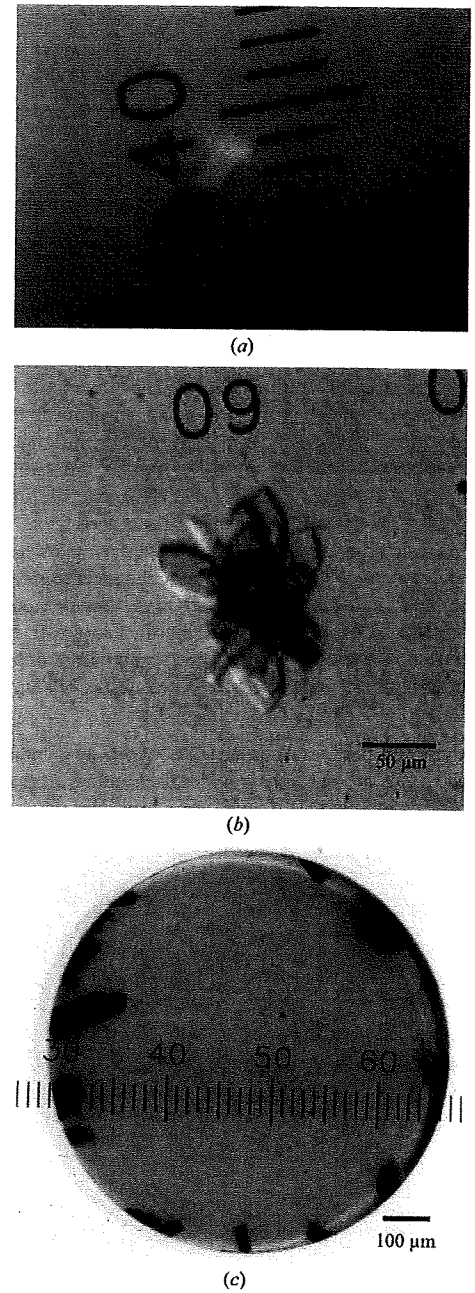

(*a*)

(*b*)

(*c*)

Figure 2
Typical crystals of *A. suum* QFR. Crystals of *A. suum* QFR obtained (*a*) by the hanging-drop vapour-diffusion method using C12E8 as the main detergent and C12M as the additive detergent, (*b*) using a 3:2 weight ratio of C12E8 and C12M and (*c*) after detergent exchange to the 3:2 C12E8:C12M mixture by microdialysis.